

Hanford Geophysical Logging Project

**2001 Recalibration of Logging Systems
for Characterization of Subsurface Contamination
at the Hanford Site**

April 2002

Prepared for
U.S. Department of Energy
Idaho Operations Office
Grand Junction Office
Grand Junction, Colorado

Prepared by
MACTEC-ERS
Grand Junction Office
Grand Junction, Colorado

Approved for public release; distribution is unlimited.
Work performed under DOE Contract No. DE-AC04-94AL96907.

Contents

	Page
Signature Page.....	iv
1.0 Introduction	1
2.0 Spectral Gamma-Ray Logging Systems	3
2.1 Calibration.....	3
2.2 Linearity Demonstration.....	18
2.3 Revised Field Verification Criteria	22
3.0 Neutron-Neutron System Calibration	26
3.1 Operation.....	26
3.2 Calibration Standards.....	26
3.3 Calibration Data.....	27
3.4 Calibration Results.....	28
3.5 Comparison to Earlier Calibrations	33
3.6 Effect of a Plastic Sleeve Covering the Sonde.....	35
3.7 Effect of a 4.0-in.-Diameter, 0.25-in.-Thick Steel Casing Inside of a 6-in. Casing.....	35
3.8 Limitations	35
4.0 Summary	38
4.1 Spectral Gamma Logging System (SGLS)	38
4.2 Neutron-Neutron	46
5.0 Acknowledgements	48
6.0 References	49
Appendix A. Revised Corrections for Steel Casing.....	A-1
B. Revised Corrections for Water-Filled Boreholes	B-1

Tables

Table 1-1. Sonde Information.....	2
2-1. Calibration Standard Source Concentrations	3
2-2. Yields of Gamma Rays Used for Calibration	5
2-3. Gamma-Ray Intensities of the Calibration Standards	6
2-4. Weighted Average Peak Intensities for Gamma 2A	8
2-5. Weighted Average Peak Intensities for Gamma 2B.....	9
2-6. Weighted Average Peak Intensities for Gamma 1D	10

Contents (continued)

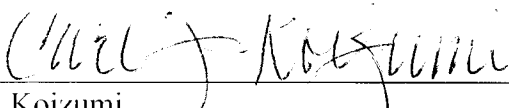
	Page
Table 2-7. SGLS $I(E)$ Values at Representative Energies	12
2-8. The 2001 Calibration Values Compared to the Previous Values	16
2-9. Representative $I(E)$ Values Calculated with the Previous and New Calibration Functions	18
2-10. Constants for the Dead Time Correction	19
2-11. Gamma 2A Field Verification Criteria	24
2-12. Gamma 2B Field Verification Criteria	25
2-13. Gamma 1D Field Verification Criteria	25
3-1. Properties of the Calibration Standards	26
3-2. Calibration Count Rate Data	28
3-3. Examples of Calculated VF and Uncertainty Values	37
4-1. Symbols, Functions and Quantities, and Customary Units	38
4-2. Field Verification Criteria for Gamma 2A	40
4-3. Field Verification Criteria for Gamma 2B	40
4-4. Field Verification Criteria for Gamma 1D	41
4-5. Constants for SGLS Dead Time Corrections	41
4-6. Constants for the Tungsten Shield Correction	42
4-7. Examples of Shield Corrections	43

Figures

Figure 2-1. Calibration Data and Calibration Function for Gamma 2A	14
2-2. Calibration Data and Calibration Function for Gamma 2B	14
2-3. Calibration Data and Calibration Function for Gamma 1D	15
2-4. Calibration Comparisons for Gamma 2A	16
2-5. Calibration Comparisons for Gamma 2B	17
2-6. Calibration Comparisons for Gamma 1D	17
2-7. Linearity Demonstration for Gamma 2A and the 295.2-keV Gamma-Ray Peak	20
2-8. Linearity Demonstration for Gamma 2A and the 609.3-keV Gamma-Ray Peak	20
2-9. Linearity Demonstration for Gamma 2B and the 352.0-keV Gamma-Ray Peak	21
2-10. Linearity Demonstration for Gamma 2B and the 1764.5-keV Gamma-Ray Peak	21
2-11. Linearity Demonstration for Gamma 1D and the 609.3-keV Gamma-Ray Peak	22
3-1. November 2001 Calibration Curve for the 6-in. Casing	30
3-2. November 2001 Calibration Curve for the 8-in. Casing	30
3-3. May 2001 Calibration Curve for the 6-in. Casing	32
3-4. May 2001 Calibration Curve for the 8-in. Casing	33
3-5. The 6-in. Casing Calibration Functions	34
3-6. The 8-in. Casing Calibration Functions	34

2001 Recalibration of Logging Systems for Characterization of Subsurface Contamination at the Hanford Site

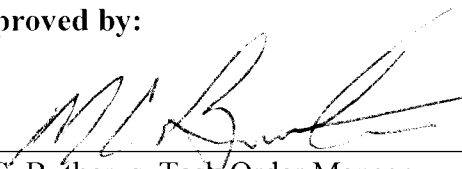
Prepared by:



C.J. Koizumi
MACTEC-ERS, Grand Junction Office

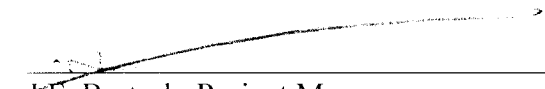
05 04 1002
Date

Approved by:



M.C. Butherus, Task Order Manager
MACTEC-ERS, Grand Junction Office

5/7/02
Date



J.F. Bertsch, Project Manager
MACTEC-ERS, Hanford

5/9/02
Date

1.0 Introduction

During 1995-2000, the U.S. Department of Energy Grand Junction Office (DOE-GJO) logged hundreds of existing boreholes around the single-shell tanks (SSTs) at DOE's Hanford Site near Richland, Washington. Log data were used to develop a baseline characterization of the gamma-ray-emitting radionuclides that are constituents of the radioactive waste that exists in the vadose zone sediments beneath and around the SSTs. In 2001, the baseline characterization effort was extended to other waste sites in the Hanford 200 Areas. This activity is supported by the DOE Richland Operations Office (DOE-RL) and the Office of River Protection (DOE-ORP).

Documents describing past and current characterization activities are posted at the Internet address <http://www.gjo.doe.gov/programs/hanf/HTFVZ.html>.

Log data consist of high resolution gamma-ray spectra acquired by passive measurements with two types of high-purity germanium (HPGe) detectors. Spectral gamma-ray logging systems (SGLSs) have sondes equipped with 35-percent-efficient, p-type, coaxial HPGe detectors (DOE 1995). For cesium-137 (^{137}Cs), which is by far the most widespread radioactive contaminant at Hanford, SGLSs acquire spectra suitable for concentration determinations over a concentration range from a fraction of a picocurie per gram (pCi/g)¹ to about 20,000 pCi/g. When concentrations exceed about 20,000 pCi/g, the SGLS detectors became "saturated," meaning that the logging systems are unable to record spectra with distinct full energy peaks.

In 1999, DOE-GJO deployed a High Rate Logging System (HRLS) to acquire spectral data from subsurface zones within which the gamma-ray intensities exceed the SGLS upper limits. The HRLS detector is a low efficiency planar 6-millimeter (mm) by 8-mm n-type HPGe detector. The HRLS acquires useful spectra for ^{137}Cs concentrations up to about 100 million picocuries per gram. More recently, a 70-percent-efficient HPGe detector and a boron trifluoride neutron detector have been added to the hardware inventory. The 70-percent detector is used when the gamma-ray signals are faint, and the boron trifluoride detector is mounted, along with an americium-beryllium neutron source, in a sonde that responds to formation moisture.

To support ongoing SST monitoring measurements and new logging assignments, logging systems are periodically recalibrated. Each system is a specific combination of logging vehicle and sonde. There are two vehicles, with names and identification numbers as follows:

Gamma 1, DOE vehicle number HO68B3572

Gamma 2, DOE vehicle number HO68B3574

The vehicle names and identification numbers have never been altered. However, because the acquisition of new sondes made many vehicle-sonde combinations possible, each sonde has been assigned a name that, in combination with the vehicle name, will identify the logging system unambiguously. The names of the sondes are indicated in Table 1-1.

¹ A picocurie is 10^{-12} of a curie, and a curie is a decay rate of 3.7×10^{10} decays per second.

Table 1-1. Sonde Information

Type of Detector	Serial Number	Original Name	New Name
35-percent-efficient HPGe	34TP20893A	Gamma 1A (was formerly used exclusively with Gamma 1)	Detector A
35-percent-efficient HPGe	36TP21095A	Backup Sonde (was formerly used with either Gamma 1 or Gamma 2)	Detector B
35-percent-efficient HPGe	34TP11019B	Gamma 2A (was formerly used exclusively with Gamma 2)	Detector D
Planar 6-mm by 8-mm HPGe	39-A314	HRLS (High Rate Logging System)	Detector C
70-percent-efficient HPGe	34TP40587A	RLS-1	Detector E
Boron trifluoride	H380932510	(none)	Detector F

Detectors A and D are the original SGLS detectors. Detector B was acquired to serve as a “backup” (spare) detector. Detector C is a low efficiency HPGe detector, and Detector E is a high efficiency HPGe detector. Detector F is a component in a logging device that responds to moisture in the subsurface.

In the past, when there were only three detectors (now named A, D, and B), logging system names indicated the vehicle and the detector, as follows. Detector A was used exclusively with vehicle Gamma 1, and the system was named “Gamma 1A.” Detector D was used exclusively with Gamma 2, and the system was named “Gamma 2A.” Although Gamma 1A and Gamma 2A had different detectors, both system names bore the letter “A.” This designation indicated simply that a system had the sonde with the original detector, not the backup detector. The systems with the backup detector were named “Gamma 1B” and “Gamma 2B.” To prevent confusion, the combinations Gamma 1 + Detector D and Gamma 2 + Detector A were not used.

Each logging system now has a name that combines the vehicle name with the new detector name. For example, “Gamma 2A” refers to Gamma 2 with the sonde that has Detector A. Because a concise and unambiguous name for this system could not be derived from the old system names, this useful combination was not used until the new detector names were assigned.

Three spectral gamma-ray logging systems (Gamma 2A, 2B, and 1D) and one neutron-neutron system (Gamma 2F) were recalibrated in 2001.

Recalibrations for the SGLSs involve five topics: (1) revised values for the constants in the calibration functions; (2) “linearity” demonstrations (which confirm the validity of the dead time corrections); (3) revised field verification criteria; (4) revised casing corrections; and (5) revised corrections for water-filled boreholes. The recalibration for the neutron-neutron system involves the revised values for the constants in the calibration function.

For the data analysts’ convenience, the recalibration results and previously derived results for

dead time corrections, casing corrections, tungsten shield corrections, and borehole water corrections are all presented in Section 4.0 of this report.

2.0 Spectral Gamma-Ray Logging Systems

2.1 Calibration

2.1.1 Calibration Standards

Calibration standards for borehole gamma-ray sensors are located at the Hanford Site calibration center, which is located near the Meteorology Station, north of the main entrance to the 200 West Area. Steele and George (1986) and Heistand and Novak (1984) describe these calibration standards and their links to radiation counting standards certified by the New Brunswick Laboratory. The references refer to the eight calibration standards as the “Spokane SBL/SBH (a pair of standards named SBL and SBH), SBT/SBK, SBU/SBM, and SBA/SBB Models.” “Spokane” refers to the original installation of these standards by DOE-GJO in the early 1980s at a calibration facility near Spokane, Washington.

Each standard is a cylindrical block of concrete with a 4.5-inch (in.)-diameter test hole coincident with the cylinder axis. The dimensions of the standards (4 feet [ft] or 5 ft in diameter, 4 ft thick) are large enough to simulate an “infinite medium,” meaning that the gamma-ray flux within the test hole at the center of a standard is indistinguishable from the flux that would exist if the medium had the same gamma-ray source concentration, but were infinite in extent.

The concrete in each standard has particular concentrations of orthoclase feldspar, uraninite, and monazite. Orthoclase feldspar contains potassium, of which about 0.01 percent is potassium-40 (^{40}K), uraninite contains uranium-238 (^{238}U) and uranium-235 (^{235}U) and the members of the uranium and actinium decay series, and monazite contains thorium-232 (^{232}Th) and the members of the thorium decay series. The “concentrations” (actually, decay rates per unit mass) of the gamma-ray sources are displayed in Table 2-1 (from Steele and George 1986).

Table 2-1. Calibration Standard Source Concentrations

Standard	^{40}K Concentration (pCi/g)	^{226}Ra Concentration ¹ (pCi/g)	^{232}Th Concentration (pCi/g)
SBK	53.50 ± 1.67	1.16 ± 0.11	0.11 ± 0.02
SBU	10.72 ± 0.84	190.52 ± 5.81	0.66 ± 0.06
SBT	10.63 ± 1.34	10.02 ± 0.48	58.11 ± 1.44
SBM	41.78 ± 1.84	125.79 ± 4.00	39.12 ± 1.07
SBA	undetermined	61.2 ± 1.7	undetermined
SBL	undetermined	324 ± 9	undetermined
SBB	undetermined	902 ± 27	undetermined
SBH	undetermined	3126 ± 180	undetermined

¹ Radium-226 is the fifth decay product of ²³⁸U. If ²²⁶Ra is in decay equilibrium with ²³⁸U, then the concentrations (decay rates per unit mass) of the two nuclides are equal. The ²²⁶Ra concentration is often cited instead of the ²³⁸U concentration because most gamma-ray-based assays utilize gamma rays that originate in nuclides that are below ²²⁶Ra in the uranium decay chain.

Calibration data were acquired using standards SBK, SBU, SBT, and SBM. Standards SBU, SBT, SBM, SBA, SBL, and SBB were used for the linearity measurements that validate the dead time corrections. Standard SBH has too high a gamma-ray intensity and was not used.

The undetermined concentrations of ⁴⁰K and ²³²Th for SBA, SBL, and SBB impose no limitations on the linearity measurements because the nuclides in the uranium series provide many gamma rays over an ample range of energies for the linearity tests.

Although the calibration standards contain potassium, uranium, and thorium, the calibrations are not specific to any of these gamma-ray sources. A system calibration relates the intensity of any spectral full energy peak to the source intensity of the corresponding gamma ray, in gamma rays per second per gram of standard material. The spectral full energy peak intensities are calculated from calibration data, and the associated gamma-ray source intensities for the calibration standards have been calculated from the known potassium, uranium, and thorium concentrations. ⁴⁰K, ²³⁵U, and ²³⁸U and the decay progenies of ²³⁸U, and ²³²Th and its decay progenies provide many gamma rays over an ample range of energies for calibration purposes.

A gamma-ray source intensity is calculated by multiplying the source concentration by two factors: the gamma ray yield (number of gamma rays emitted per decay) and the conversion factor 3.7×10^{-2} disintegrations per second per picocurie per gram.

The gamma-ray yield values published by Firestone (1996, 1999) have been used. These values are listed in Table 2-2.

Table 2-2. Yields of Gamma Rays Used for Calibration

First Nuclide in Decay Chain	Source Nuclide	Gamma-Ray Energy (keV)	Gamma-Ray Yield ($\gamma/100D$) ¹
Th-232	Ac-228	129.065	2.45
U-235 ²	U-235	185.715	2.634
U-238	Ra-226	186.100	3.50
Th-232	Pb-212	238.632	43.30
U-235 ²	Ra-223	269.459	0.631
Th-232	Ac-228	270.243	3.43
U-238	Pb-214	295.213	18.50
Th-232	Ac-228	327.995	2.953
Th-232	Ac-228	338.322	11.252
U-235 ²	Bi-211	351.06	0.595
U-238	Pb-214	351.921	35.80
Th-232	Ac-228	409.46	1.936
U-238	Pb-214	462.10	0.23
Th-232	Ac-228	463.005	4.442
Th-232	Tl-208 ³	583.191	30.364
Th-232	Ac-228	583.41	0.114
U-238	Bi-214	609.312	44.791
Th-232	Ac-228	726.863	0.638
Th-232	Bi-212	727.33	6.579
U-238	Bi-214	768.356	4.799
Th-232	Bi-212	785.37	1.102
U-238	Pb-214	785.91	0.851
U-238	Bi-214	786.1	0.30
Th-232	Ac-228	794.947	4.336
Th-232	Ac-228	835.7	1.676
Th-232	Tl-208 ³	860.564	4.465
Th-232	Ac-228	911.205	26.60
U-238	Bi-214	934.061	3.029
U-238	Bi-214	964.08	0.38
Th-232	Ac-228	964.77	5.107
Th-232	Ac-228	968.971	16.173
U-238	Pa-234m	1001.0	0.837
U-238	Bi-214	1120.287	14.797
U-238	Bi-214	1155.19	1.64
U-238	Bi-214	1238.11	5.859
U-238	Bi-214	1377.669	3.919
U-238	Bi-214	1407.98	2.799
Th-232	Ac-228	1459.14	0.798
K-40	K-40	1460.83	10.67
U-238	Bi-214	1509.228	2.12
Th-232	Ac-228	1588.21	3.272
Th-232	Bi-212	1620.5	1.486
U-238	Bi-214	1729.595	2.879

First Nuclide in Decay Chain	Source Nuclide	Gamma-Ray Energy (keV)	Gamma-Ray Yield (γ/100D) ¹
U-238	Bi-214	1764.494	15.357
U-238	Bi-214	1847.42	2.04
U-238	Bi-214	2204.21	4.859
U-238	Bi-214	2447.86	1.5
Th-232	Tl-208 ³	2614.533	35.64

¹ The yield unit is gamma rays per 100 decays.

² Yields for ²³⁵U and its decay products are expressed in gamma rays per 100 decays of ²³⁸U.

³ All of the ²⁰⁸Tl gamma-ray yields have been adjusted for the ²¹²Bi alpha decay branching ratio. The Firestone (1999) value for the ratio (0.3594) was used.

Table 2-3 lists the gamma-ray intensities that were calculated with the calibration standard source concentrations in Table 2-1 and the gamma-ray yields in Table 2-2.

Table 2-3. Gamma-Ray Intensities of the Calibration Standards

	SBK	SBU	SBT	SBM
Energy (keV)	Total Intensity (γ/s/g) ¹	Total Intensity (γ/s/g)	Total Intensity (γ/s/g)	Total Intensity (γ/s/g)
129.1	1.00E-04 ± 1.8E-05	7.16E-04 ± 6.5E-05	6.30E-02 ± 1.6E-03	4.24E-02 ± 1.2E-03
185.7, 186.0 ²	2.63E-03 ± 1.8E-04	4.14E-01 ± 9.0E-03	2.18E-02 ± 7.4E-04	2.73E-01 ± 6.2E-03
238.6	1.76E-03 ± 3.2E-04	1.05E-02 ± 9.6E-04	9.27E-01 ± 2.3E-02	6.24E-01 ± 1.7E-02
269.5, 270.2	4.09E-04 ± 3.6E-05	4.70E-02 ± 1.4E-03	8.35E-02 ± 2.0E-03	8.50E-02 ± 1.8E-03
295.2	7.95E-03 ± 7.5E-04	1.35E+00 ± 4.1E-02	7.12E-02 ± 3.4E-03	8.94E-01 ± 2.8E-02
328.0	1.21E-04 ± 2.2E-05	8.21E-04 ± 7.5E-05	7.22E-02 ± 1.8E-03	4.86E-02 ± 1.3E-03
338.3	4.58E-04 ± 8.3E-05	2.93E-03 ± 2.7E-04	2.58E-01 ± 6.4E-03	1.74E-01 ± 4.8E-03
351.1, 351.9	1.56E-02 ± 1.5E-03	2.66E+00 ± 8.0E-02	1.40E-01 ± 6.6E-03	1.75E+00 ± 5.5E-02
409.5	7.9E-5 ± 1.4E-5	4.73E-4 ± 4.3E-5	4.16E-2 ± 1.0E-3	2.802E-2 ± 7.7E-4
462.1, 463.0	2.81E-04 ± 3.4E-05	1.31E-02 ± 3.8E-04	1.00E-01 ± 2.5E-03	7.51E-02 ± 1.9E-03
583.2, 583.4	1.25E-03 ± 2.3E-04	7.61E-03 ± 6.9E-04	6.70E-01 ± 1.7E-02	4.51E-01 ± 1.2E-02
609.3	1.92E-02 ± 1.8E-03	3.25E+00 ± 9.9E-02	1.71E-01 ± 8.2E-03	2.15E+00 ± 6.8E-02
726.9, 727.3	4.45E-04 ± 7.6E-05	1.82E-03 ± 1.5E-04	1.60E-01 ± 3.6E-03	1.08E-01 ± 2.7E-03
768.4	2.06E-03 ± 2.0E-04	3.44E-01 ± 1.0E-02	1.81E-02 ± 8.7E-04	2.27E-01 ± 7.2E-03
785.4, 785.9, 786.1	5.68E-04 ± 3.9E-05	9.92E-02 ± 2.4E-03	2.90E-02 ± 6.2E-04	9.43E-02 ± 1.9E-03
794.9	1.77E-04 ± 3.2E-05	1.12E-03 ± 1.0E-04	9.89E-02 ± 2.5E-03	6.66E-02 ± 1.8E-03
835.7	6.8E-5 ± 1.2E-5	4.09E-4 ± 3.7E-5	3.604E-2 ± 8.9E-4	2.426E-2 ± 6.6E-4
860.6	1.83E-04 ± 3.3E-05	1.05E-03 ± 9.6E-05	9.29E-02 ± 2.3E-03	6.25E-02 ± 1.7E-03
911.2	1.08E-03 ± 2.0E-04	7.08E-03 ± 6.4E-04	6.24E-01 ± 1.5E-02	4.20E-01 ± 1.1E-02
934.1	1.30E-03 ± 1.2E-04	2.23E-01 ± 6.8E-03	1.18E-02 ± 5.6E-04	1.48E-01 ± 4.7E-03
964.1, 964.8	3.73E-04 ± 4.1E-05	2.84E-02 ± 8.3E-04	1.26E-01 ± 3.1E-03	1.02E-01 ± 2.4E-03

	SBK	SBU	SBT	SBM
Energy (keV)	Total Intensity (γ/s/g)¹	Total Intensity (γ/s/g)	Total Intensity (γ/s/g)	Total Intensity (γ/s/g)
969.0	6.58E-04 \pm 1.2E-04	4.26E-03 \pm 3.9E-04	3.75E-01 \pm 9.3E-03	2.53E-01 \pm 6.9E-03
1001.0	3.60E-4 \pm 3.4E-5	5.92E-2 \pm 1.8E-3	3.11E-3 \pm 1.5E-4	3.91E-2 \pm 1.2E-3
1120.3	6.36E-03 \pm 6.0E-04	1.06E+00 \pm 3.2E-02	5.58E-02 \pm 2.7E-03	7.00E-01 \pm 2.2E-02
1155.2	7.04E-4 \pm 6.7E-5	1.156E-1 \pm 3.5E-3	6.08E-3 \pm 2.9E-4	7.63E-2 \pm 2.4E-3
1238.1	2.52E-03 \pm 2.4E-04	4.17E-01 \pm 1.3E-02	2.19E-02 \pm 1.1E-03	2.76E-01 \pm 8.8E-03
1377.7	1.69E-03 \pm 1.6E-04	2.83E-01 \pm 8.6E-03	1.49E-02 \pm 7.1E-04	1.87E-01 \pm 5.9E-03
1408	1.22E-03 \pm 1.2E-04	1.75E-01 \pm 5.3E-03	9.19E-03 \pm 4.4E-04	1.15E-01 \pm 3.7E-03
1459.1, 1460.8	2.11E-01 \pm 6.6E-03	4.27E-02 \pm 3.3E-03	6.44E-02 \pm 5.3E-03	1.80E-01 \pm 7.3E-03
1509.2	9.12E-04 \pm 8.6E-05	1.54E-01 \pm 4.7E-03	8.12E-03 \pm 3.9E-04	1.02E-01 \pm 3.2E-03
1588.2	1.34E-04 \pm 2.4E-05	9.06E-04 \pm 8.2E-05	7.74E-02 \pm 1.9E-03	5.37E-02 \pm 1.5E-03
1620.5	9.46E-05 \pm 1.7E-05	3.69E-04 \pm 3.4E-05	3.25E-02 \pm 8.0E-04	2.19E-02 \pm 6.0E-04
1729.6	1.24E-03 \pm 1.2E-04	2.15E-01 \pm 6.6E-03	1.13E-02 \pm 5.4E-04	1.42E-01 \pm 4.5E-03
1764.5	6.59E-03 \pm 6.3E-04	1.12E+00 \pm 3.4E-02	5.90E-02 \pm 2.8E-03	7.41E-01 \pm 2.4E-02
1847.4	8.77E-04 \pm 8.3E-05	1.49E-01 \pm 4.6E-03	7.86E-03 \pm 3.8E-04	9.87E-02 \pm 3.1E-03
2204.2	2.09E-03 \pm 2.0E-04	3.52E-01 \pm 1.1E-02	1.85E-02 \pm 8.9E-04	2.32E-01 \pm 7.4E-03
2447.9	6.44E-4 \pm 6.1E-5	1.057E-1 \pm 3.2E-3	5.56E-3 \pm 2.7E-4	6.98E-2 \pm 2.2E-3
2614.5	1.46E-03 \pm 2.7E-04	8.79E-03 \pm 8.0E-04	7.74E-01 \pm 1.9E-02	5.21E-01 \pm 1.4E-02

¹ Gamma rays per second per gram of material.

² Multiple energy entries indicate energies that differ by such small amounts that the peaks cannot be resolved. When the peaks for several gamma rays with similar energies can't be resolved, the analysis software treats the composite signal as one peak, and reports one peak intensity.

2.1.2 Calibration Measurements

Six or more spectra per calibration standard were recorded under the following conditions:

- No casing in test hole.
- No liquid in test hole.
- Sonde centered in test hole (sonde cylindrical axis coincident with borehole axis).
- Detector held stationary at depth corresponding to center of calibration standard.

The counting time was 1,000 seconds per spectrum.

Variations in the borehole diameter generally do not influence the gamma-ray fluxes incident on the sonde if the borehole contains no liquid. Most of the logging at Hanford occurs in dry boreholes; therefore, it is unimportant that the test holes in the calibration standards have smaller diameters (4.5 in.) than most Hanford boreholes (6.0 in., nominal). In the rare cases when a borehole contains water, corrections can be applied (DOE 1995; Koizumi 2000).

Whereas the calibration standard test holes are “open” (have no casing), Hanford boreholes are all lined with steel casing. Corrections for casing of various thicknesses have been derived (DOE 1995; Koizumi 2000) and are described in Section 4.1.3.3 of this report.

2.1.3 Calibration Data

The calibration spectra were analyzed with the spectrum analysis program *PCMCA/WIN* (Version 6.3.1, release 13, Aptec Engineering Limited, North Tonawanda, New York). The program has two algorithms, *peaksearch* and *multifit*, that identify full energy peaks and calculate the peak areas (intensities). *Peaksearch* finds peak-like features in spectra; *multifit* performs tests to separate peaks from spurious features, then fits a Gaussian distribution function and a background function to each peak. The peak intensity is the integral of the Gaussian distribution function, less background. The *Hanford Geophysical Logging Project Data Analysis Manual* (revision in progress) presents brief descriptions of these calculations.

Tables 2-4, 2-5, and 2-6 display full energy peak intensities from the calibration spectra. Each peak intensity is the weighted average of the intensities from the group of spectra for the standard designated at the top of the column. The intensities have all been corrected for dead time, as described in Section 4.1.3.1 of this report.

Table 2-4. Weighted Average Peak Intensities for Gamma 2A

Representative Gamma-Ray Energy (keV)	SBK Peak Intensities (c/s) ¹	SBU Peak Intensities (c/s)	SBT Peak Intensities (c/s)	SBM Peak Intensities (c/s)
129.1	no data	no data	no data	5.3 ± 1.5
185.9	no data	40.90 ± 0.56	no data	27.46 ± 0.47
238.6	no data	no data	no data	64.9 ± 7.2
269.9	no data	4.89 ± 0.46	no data	7.01 ± 0.36
295.2	0.726 ± 0.043	119.9 ± 1.3	6.26 ± 0.23	77.6 ± 1.3
328.0	no data	no data	5.28 ± 0.26	2.84 ± 0.45
338.3	no data	no data	20.85 ± 0.33	14.40 ± 0.43
351.5	1.430 ± 0.051	224.4 ± 2.7	12.00 ± 0.23	148.2 ± 1.2
409.5	no data	no data	3.19 ± 0.13	no data
462.6	no data	no data	7.35 ± 0.16	4.87 ± 0.19
583.3	no data	no data	45.45 ± 0.55	30.72 ± 0.30
609.3	1.354 ± 0.042	227.6 ± 3.0	12.24 ± 0.19	149.8 ± 1.3
727.1	no data	no data	10.39 ± 0.13	7.00 ± 0.19
768.4	no data	24.38 ± 0.35	no data	15.64 ± 0.43
785.8	no data	5.59 ± 0.14	1.56 ± 0.12	4.45 ± 0.13
795.0	no data	no data	6.21 ± 0.17	4.13 ± 0.13
835.7	no data	no data	2.328 ± 0.072	no data
860.6	no data	no data	6.25 ± 0.10	4.15 ± 0.14
911.2	no data	no data	36.18 ± 0.31	24.73 ± 0.26
934.1	no data	14.13 ± 0.20	0.716 ± 0.058	9.32 ± 0.15
964.4	no data	1.60 ± 0.11	6.68 ± 0.16	5.36 ± 0.13
969.0	no data	no data	21.89 ± 0.26	14.84 ± 0.17

Representative Gamma-Ray Energy (keV)	SBK Peak Intensities (c/s)¹	SBU Peak Intensities (c/s)	SBT Peak Intensities (c/s)	SBM Peak Intensities (c/s)
1001.0	no data	4.09 ± 0.10	no data	2.67 ± 0.10
1120.3	0.386 ± 0.027	66.18 ± 0.60	3.613 ± 0.065	43.51 ± 0.42
1155.2	no data	7.34 ± 0.13	0.50 ± 0.042	4.83 ± 0.10
1238.1	no data	25.29 ± 0.20	1.378 ± 0.048	16.70 ± 0.17
1377.7	no data	17.50 ± 0.15	0.893 ± 0.041	11.55 ± 0.12
1408.0	no data	10.17 ± 0.11	0.542 ± 0.042	6.64 ± 0.10
1460.8	12.88 ± 0.15	2.551 ± 0.083	3.28 ± 0.14	10.79 ± 0.12
1509.2	0.050 ± 0.013	8.86 ± 0.14	0.479 ± 0.047	5.80 ± 0.13
1588.2	no data	no data	3.832 ± 0.075	2.75 ± 0.12
1620.5	no data	no data	1.880 ± 0.080	1.184 ± 0.076
1729.6	0.0618 ± 0.0070	12.07 ± 0.12	0.591 ± 0.030	7.905 ± 0.092
1764.5	0.364 ± 0.017	63.51 ± 0.67	3.354 ± 0.063	41.61 ± 0.39
1847.4	0.0425 ± 0.0069	8.26 ± 0.12	0.402 ± 0.034	5.424 ± 0.087
2204.2	0.0990 ± 0.0085	18.83 ± 0.17	0.960 ± 0.037	12.26 ± 0.15
2447.9	0.0163 ± 0.0033	5.755 ± 0.088	0.327 ± 0.030	3.678 ± 0.066
2614.5	0.0595 ± 0.0067	0.392 ± 0.026	36.55 ± 0.25	24.75 ± 0.25

¹ counts per second.

Table 2-5. Weighted Average Peak Intensities for Gamma 2B

Representative Gamma-Ray Energy (keV)	SBK Peak Intensities (c/s)	SBU Peak Intensities (c/s)	SBT Peak Intensities (c/s)	SBM Peak Intensities (c/s)
129.1	no data	no data	no data	4.12 ± 0.94
185.9	no data	39.07 ± 0.53	no data	24.87 ± 0.32
238.6	no data	no data	no data	53.9 ± 1.1
269.9	no data	4.62 ± 0.54	no data	6.71 ± 0.28
295.2	0.751 ± 0.037	116.8 ± 1.0	6.06 ± 0.18	73.8 ± 1.0
328.0	no data	no data	5.06 ± 0.16	3.04 ± 0.24
338.3	no data	no data	19.22 ± 0.27	13.10 ± 0.31
351.5	1.359 ± 0.036	221.5 ± 2.1	11.58 ± 0.16	139.9 ± 1.7
409.5	no data	no data	3.212 ± 0.095	no data
462.6	no data	no data	6.93 ± 0.10	5.04 ± 0.14
583.3	no data	no data	44.09 ± 0.39	29.46 ± 0.44
609.3	1.356 ± 0.040	230.8 ± 2.8	11.71 ± 0.12	145.0 ± 1.5
727.1	no data	no data	10.36 ± 0.10	6.72 ± 0.14
768.4	no data	24.14 ± 0.48	1.012 ± 0.083	14.60 ± 0.28
785.8	no data	5.48 ± 0.14	1.49 ± 0.10	4.34 ± 0.15
795.0	no data	no data	5.978 ± 0.094	3.91 ± 0.14
835.7	no data	no data	2.303 ± 0.073	1.08 ± 0.21
860.6	no data	no data	6.120 ± 0.069	4.041 ± 0.090
911.2	no data	no data	36.04 ± 0.26	23.75 ± 0.22
934.1	no data	14.27 ± 0.15	0.731 ± 0.042	9.14 ± 0.16
964.4	no data	1.45 ± 0.14	6.82 ± 0.15	5.27 ± 0.13

Representative Gamma-Ray Energy (keV)	SBK Peak Intensities (c/s)	SBU Peak Intensities (c/s)	SBT Peak Intensities (c/s)	SBM Peak Intensities (c/s)
969.0	no data	no data	21.74 ± 0.25	14.45 ± 0.17
1001.0	no data	4.07 ± 0.11	no data	2.655 ± 0.088
1120.3	0.396 ± 0.021	68.44 ± 0.66	3.459 ± 0.053	43.09 ± 0.43
1155.2	no data	7.52 ± 0.10	0.481 ± 0.042	4.713 ± 0.088
1238.1	no data	26.29 ± 0.20	1.300 ± 0.044	16.43 ± 0.16
1377.7	no data	18.32 ± 0.21	0.933 ± 0.045	11.63 ± 0.11
1408.0	no data	10.35 ± 0.10	0.526 ± 0.041	6.54 ± 0.10
1460.8	13.24 ± 0.012	2.559 ± 0.073	3.21 ± 0.15	10.78 ± 0.16
1509.2	0.060 ± 0.014	9.19 ± 0.10	0.417 ± 0.031	5.77 ± 0.12
1588.2	no data	no data	3.846 ± 0.067	2.65 ± 0.16
1620.5	no data	no data	1.884 ± 0.046	1.188 ± 0.078
1729.6	0.0623 ± 0.0063	12.58 ± 0.13	0.599 ± 0.033	7.87 ± 0.11
1764.5	0.378 ± 0.014	66.97 ± 0.78	3.301 ± 0.049	41.72 ± 0.48
1847.4	0.0398 ± 0.0052	8.67 ± 0.10	0.418 ± 0.029	5.387 ± 0.086
2204.2	0.0961 ± 0.0083	19.87 ± 0.25	1.003 ± 0.032	12.52 ± 0.14
2447.9	0.0278 ± 0.0055	6.036 ± 0.076	0.301 ± 0.029	3.794 ± 0.067
2614.5	0.0659 ± 0.0062	0.426 ± 0.022	37.30 ± 0.31	25.00 ± 0.34

Table 2-6. Weighted Average Peak Intensities for Gamma 1D

Representative Gamma-Ray Energy (keV)	SBK Peak Intensities (c/s)	SBU Peak Intensities (c/s)	SBT Peak Intensities (c/s)	SBM Peak Intensities (c/s)
129.1	no data	no data	3.26 ± 0.86	no data
185.9	no data	33.32 ± 0.38	no data	22.30 ± 0.31
209.3	no data	no data	6.15 ± 0.58	3.53 ± 0.92
238.6	no data	no data	74.0 ± 7.4	46.1 ± 8.3
241.5	no data	39.39 ± 0.72	73.7 ± 2.9	no data
269.9	no data	4.40 ± 0.73	5.43 ± 0.42	5.86 ± 0.37
277.4	no data	no data	3.55 ± 0.15	no data
295.2	0.611 ± 0.040	98.6 ± 1.3	5.54 ± 0.17	62.5 ± 1.6
328.0	no data	no data	4.68 ± 0.17	2.99 ± 0.31
338.3	no data	no data	17.46 ± 0.29	11.22 ± 0.38
351.5	1.128 ± 0.039	184.5 ± 1.8	10.14 ± 0.14	120.6 ± 1.8
409.5	no data	no data	2.83 ± 0.10	no data
462.6	no data	no data	6.08 ± 0.10	4.49 ± 0.17
583.3	no data	no data	38.11 ± 0.40	24.68 ± 0.52
609.3	1.112 ± 0.036	188.1 ± 2.2	10.08 ± 0.13	121.4 ± 1.9
727.1	no data	no data	8.719 ± 0.089	5.77 ± 0.14
768.4	no data	19.61 ± 0.35	1.008 ± 0.072	11.54 ± 0.34
785.8	no data	4.30 ± 0.12	1.343 ± 0.092	3.48 ± 0.12
795.0	no data	no data	5.059 ± 0.085	3.36 ± 0.13
835.7	no data	no data	1.845 ± 0.088	no data
860.6	no data	no data	5.158 ± 0.063	3.30 ± 0.11
911.2	no data	no data	30.34 ± 0.24	19.78 ± 0.24

Representative Gamma-Ray Energy (keV)	SBK Peak Intensities (c/s)	SBU Peak Intensities (c/s)	SBT Peak Intensities (c/s)	SBM Peak Intensities (c/s)
934.1	no data	11.53 ± 0.17	0.615 ± 0.050	7.44 ± 0.14
964.4	no data	no data	5.86 ± 0.10	4.47 ± 0.11
969.0	no data	no data	18.47 ± 0.17	12.01 ± 0.15
1001.0	no data	3.237 ± 0.095	no data	2.14 ± 0.10
1120.3	0.302 ± 0.023	54.06 ± 0.49	2.926 ± 0.058	35.18 ± 0.35
1155.2	no data	5.87 ± 0.11	no data	3.885 ± 0.073
1238.1	no data	20.80 ± 0.24	1.127 ± 0.042	13.38 ± 0.13
1377.7	no data	14.27 ± 0.14	0.739 ± 0.038	9.30 ± 0.11
1460.8	10.15 ± 0.017	2.103 ± 0.069	2.64 ± 0.14	8.53 ± 0.14
1509.2	no data	7.26 ± 0.11	0.386 ± 0.047	4.62 ± 0.10
1588.2	no data	no data	3.235 ± 0.083	2.13 ± 0.14
1620.5	no data	no data	1.508 ± 0.066	0.962 ± 0.052
1729.6	0.0494 ± 0.0061	9.72 ± 0.11	0.516 ± 0.032	6.263 ± 0.087
1764.5	0.282 ± 0.013	51.70 ± 0.58	2.772 ± 0.059	33.41 ± 0.43
1847.4	0.042 ± 0.010	6.75 ± 0.10	0.377 ± 0.036	4.277 ± 0.071
2204.2	0.0738 ± 0.0068	15.35 ± 0.18	0.811 ± 0.039	9.86 ± 0.14
2447.9	no data	4.662 ± 0.083	0.242 ± 0.043	2.975 ± 0.057
2614.5	0.0442 ± 0.0047	0.327 ± 0.023	30.11 ± 0.38	19.66 ± 0.24

2.1.4 SGLS Calibration Function

The calibration function, $I(E)$, is a function of the gamma-ray energy E and is defined as follows:

$$I(E) = \frac{\text{gamma-ray source intensity in gammas per second per gram}}{\text{intensity of the gamma-ray peak in counts per second}}. \quad \text{Eq. (2-1)}$$

With the source intensities in Table 2-3 and the peak intensities in Tables 2-4, 2-5, and 2-6, values for $I(E)$ were calculated for specific gamma-ray energies. For each logging unit, and any particular energy, up to four $I(E)$ values were determined, one for each calibration standard. For a particular logging unit and a particular energy, a representative $I(E)$ value was derived by calculating the weighted average of the $I(E)$ values for the various calibration standards. The $I(E)$ values are listed in Table 2-7.

Table 2-7. SGLS $I(E)$ Values at Representative Energies

Representative Gamma-Ray Energy (keV)	Gamma 2A $I(E)$ ((γ/s/g)/(c/s))	Gamma 2B $I(E)$ ((γ/s/g)/(c/s))	Gamma 1D $I(E)$ ((γ/s/g)/(c/s))
129.1	0.0067 ± 0.0019	0.0086 ± 0.0020	0.0130 ± 0.0022
185.9	0.01037 ± 0.00029	0.01098 ± 0.00020	0.01277 ± 0.00034
238.6	0.0097 ± 0.0011	0.01162 ± 0.00039	0.0128 ± 0.0014
269.9	0.01076 ± 0.00052	0.01150 ± 0.00050	0.01341 ± 0.00075
295.2	0.01115 ± 0.00024	0.01153 ± 0.00024	0.01325 ± 0.00045

Representative Gamma-Ray Energy (keV)	Gamma 2A <i>I(E)</i> ((γ/s/g)/(c/s))	Gamma 2B <i>I(E)</i> ((γ/s/g)/(c/s))	Gamma 1D <i>I(E)</i> ((γ/s/g)/(c/s))
328.0	0.01202 ± 0.00067	0.01255 ± 0.00050	0.01366 ± 0.00082
338.3	0.01150 ± 0.00027	0.01252 ± 0.00028	0.01406 ± 0.00038
351.5	0.01153 ± 0.00024	0.01195 ± 0.00024	0.01385 ± 0.00042
409.5	0.01305 ± 0.00061	0.01296 ± 0.00050	0.01469 ± 0.00065
462.6	0.01371 ± 0.00037	0.01424 ± 0.00032	0.01611 ± 0.00045
583.3	0.01439 ± 0.00029	0.01491 ± 0.00030	0.01745 ± 0.00039
609.3	0.01400 ± 0.00029	0.01421 ± 0.00029	0.01689 ± 0.00052
727.1	0.01493 ± 0.00032	0.01518 ± 0.00030	0.01790 ± 0.00039
768.4	0.01418 ± 0.00037	0.01487 ± 0.00037	0.01806 ± 0.00061
785.8	0.01665 ± 0.00040	0.01722 ± 0.00043	0.01959 ± 0.00062
795.0	0.01510 ± 0.00041	0.01607 ± 0.00074	0.01850 ± 0.00053
835.7	0.01548 ± 0.00061	0.01565 ± 0.00063	0.0195 ± 0.0010
860.6	0.01544 ± 0.00038	0.01600 ± 0.00056	0.01891 ± 0.00049
911.2	0.01570 ± 0.00031	0.01602 ± 0.00031	0.01911 ± 0.00038
934.1	0.01548 ± 0.00037	0.01553 ± 0.00036	0.01869 ± 0.00066
964.4	0.01695 ± 0.00039	0.01758 ± 0.00056	0.01966 ± 0.00044
969.0	0.01583 ± 0.00032	0.01620 ± 0.00048	0.01912 ± 0.00038
1001.0	0.01462 ± 0.00073	0.01473 ± 0.00068	0.01829 ± 0.00064
1120.3	0.01581 ± 0.00033	0.01573 ± 0.00036	0.01937 ± 0.00072
1155.2	0.01502 ± 0.00053	0.01554 ± 0.00054	0.01966 ± 0.00050
1238.1	0.01633 ± 0.00035	0.01626 ± 0.00035	0.02001 ± 0.00050
1377.7	0.01602 ± 0.00035	0.01557 ± 0.00036	0.01949 ± 0.00055
1408.0	0.01821 ± 0.00042	0.01811 ± 0.00042	no data
1460.8	0.01650 ± 0.00040	0.01625 ± 0.00039	0.02082 ± 0.00078
1509.2	0.01720 ± 0.00043	0.01702 ± 0.00040	0.02091 ± 0.00096
1588.2	0.01802 ± 0.00049	0.01822 ± 0.00050	0.02185 ± 0.00089
1620.5	0.01735 ± 0.00070	0.01716 ± 0.00053	0.02167 ± 0.00086
1729.6	0.01749 ± 0.00038	0.01718 ± 0.00038	0.0212 ± 0.0011
1764.5	0.01737 ± 0.00036	0.01701 ± 0.00035	0.02115 ± 0.00072
1847.4	0.01789 ± 0.00042	0.01752 ± 0.00040	0.0216 ± 0.0015
2204.2	0.01865 ± 0.00040	0.01796 ± 0.00039	0.0227 ± 0.0010
2447.9	0.01859 ± 0.00045	0.01796 ± 0.00043	0.0231 ± 0.0015
2614.5	0.02097 ± 0.00040	0.02059 ± 0.00040	0.0259 ± 0.0019

For each logging system, the energies and $I(E)$ values were analyzed with the curve fitting program *TableCurve Windows* (Version 1.11, Jandel Scientific, San Rafael, California). The analysis was constrained to fit the SGLS calibration function

$$I(E) = (A + B \cdot \ln(E))^2 \quad \text{Eq. (2-2)}$$

to the data.

A and B are the calibration constants. Their values, as determined by the curve fitting, are:

Gamma 2A

$$A = 0.0213 \pm 0.0029$$

$$B = 0.01510 \pm 0.00043$$

Gamma 2B

$$A = 0.0378 \pm 0.0028$$

$$B = 0.01275 \pm 0.00043$$

Gamma 1D

$$A = 0.0266 \pm 0.0026$$

$$B = 0.01622 \pm 0.00039.$$

These values for A and B are used with Equation (2-2) to calculate $I(E)$, in (gammas per second per gram) per (count per second), for any energy E between 129 and 2614 keV. The energy must be expressed in kilo-electron-volts.

The $I(E)$ values for Gamma 2A in Table 2-7 are depicted by small circles in the plot in Figure 2-1, and the function determined by curve fitting is represented by the smooth curve.

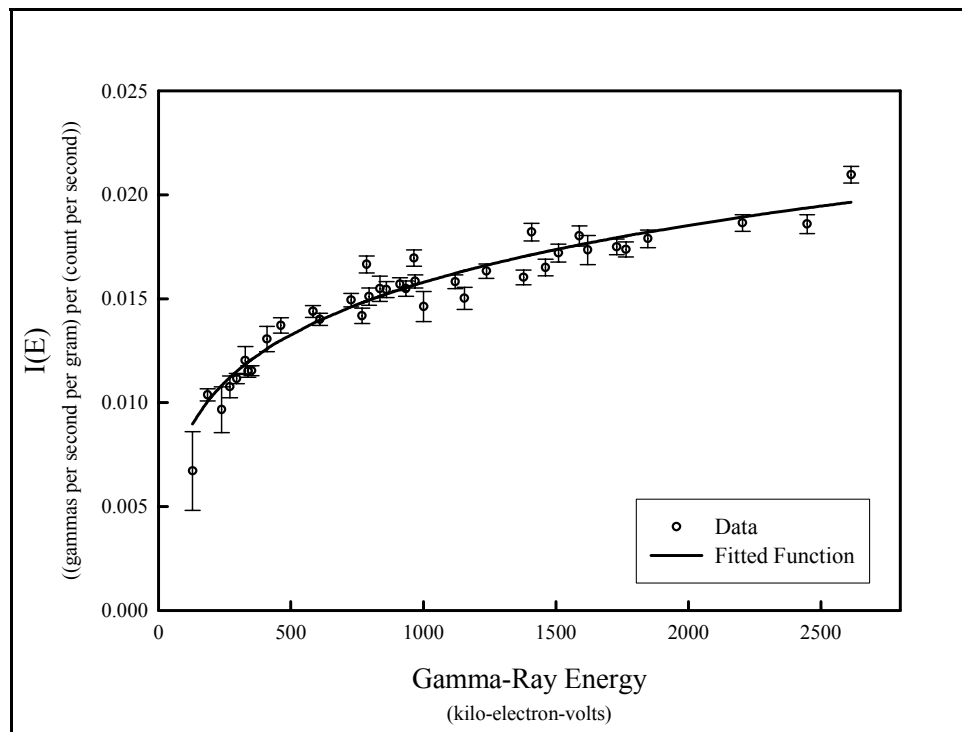


Figure 2-1. Calibration Data and Calibration Function for Gamma 2A

Small circles in Figure 2-2 depict the $I(E)$ values for Gamma 2B in Table 2-7, and the function determined by curve fitting is represented by the smooth curve.

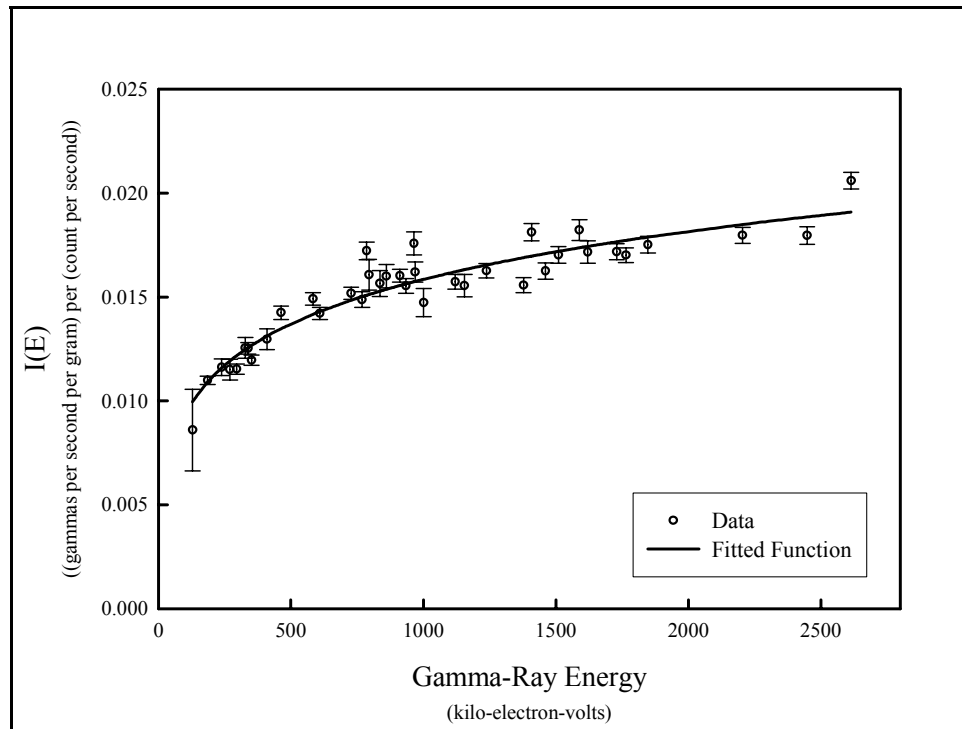


Figure 2-2. Calibration Data and Calibration Function for Gamma 2B

Figure 2-3 shows the $I(E)$ values for Gamma 1D in Table 2-7 and the function determined by curve fitting.

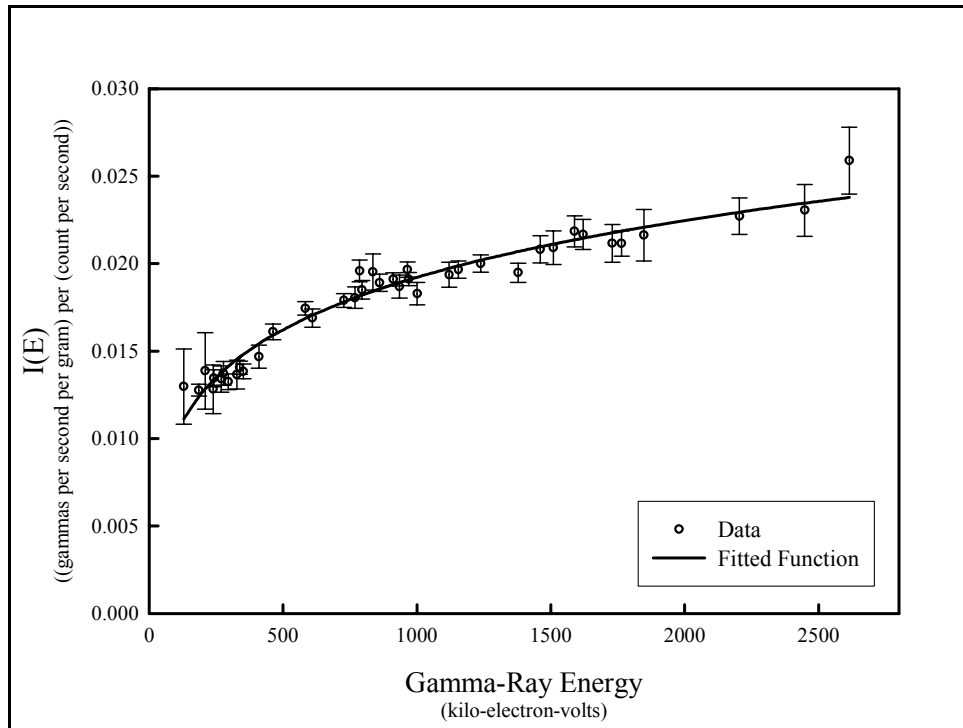


Figure 2-3. Calibration Data and Calibration Function for Gamma 1D

The calibration function is used as follows. After the logging system records a gamma-ray spectrum, the full energy peaks are analyzed with the spectrum analysis program to determine the gamma-ray energies (in kilo-electron-volts) and peak intensities (in counts per second). The energies are used, along with the calibration constants for the logging system, to determine the values of $I(E)$ corresponding to the energies.

The peak intensities are corrected for dead time, casing, and other effects, if necessary, then each corrected intensity, P , is multiplied by the associated $I(E)$ value. The result is the intensity of the gamma-ray source:

$$\text{source intensity} = S_I = P \cdot I(E). \quad \text{Eq. (2-3)}$$

To calculate the concentration of the gamma-ray source, the analyst uses

$$\text{concentration} = \frac{27.027}{Y} \cdot S_I, \quad \text{Eq. (2-4)}$$

where Y is the gamma-ray yield, in gamma rays per decay. The coefficient 27.027 is a unit conversion factor: 27.027 pCi = 1 decay per second.

Section 4.1.1 in this report describes how to calculate the concentration uncertainty.

2.1.5 Comparison of 2001 Calibrations with Previous Calibrations

Table 2-8 displays values of the 2001 calibration constants and the corresponding values from the previous calibrations.

Table 2-8. The 2001 Calibration Constant Values Compared to the Previous Values

System	Previous ¹ Values		2001 Values	
	<i>A</i>	<i>B</i>	<i>A</i>	<i>B</i>
Gamma 2A ²	0.0195 ± 0.0036	0.01524 ± 0.00054	0.0213 ± 0.0029	0.01510 ± 0.00043
Gamma 2B	0.0397 ± 0.0040	0.01272 ± 0.00059	0.0378 ± 0.0028	0.01275 ± 0.00043
Gamma 1D	0.0260 ± 0.0033	0.01659 ± 0.00050	0.0266 ± 0.0026	0.01622 ± 0.00039

¹ Detector A was previously recalibrated in August 1998; Detectors B and D were recalibrated in September 2000.

² For the 1998 calibration, Detector A was operated by Gamma 1.

Figures 2-4, 2-5, and 2-6 display graphs of the $I(E)$ values plotted in relation to E values ranging from 100 to 1332.5 keV.

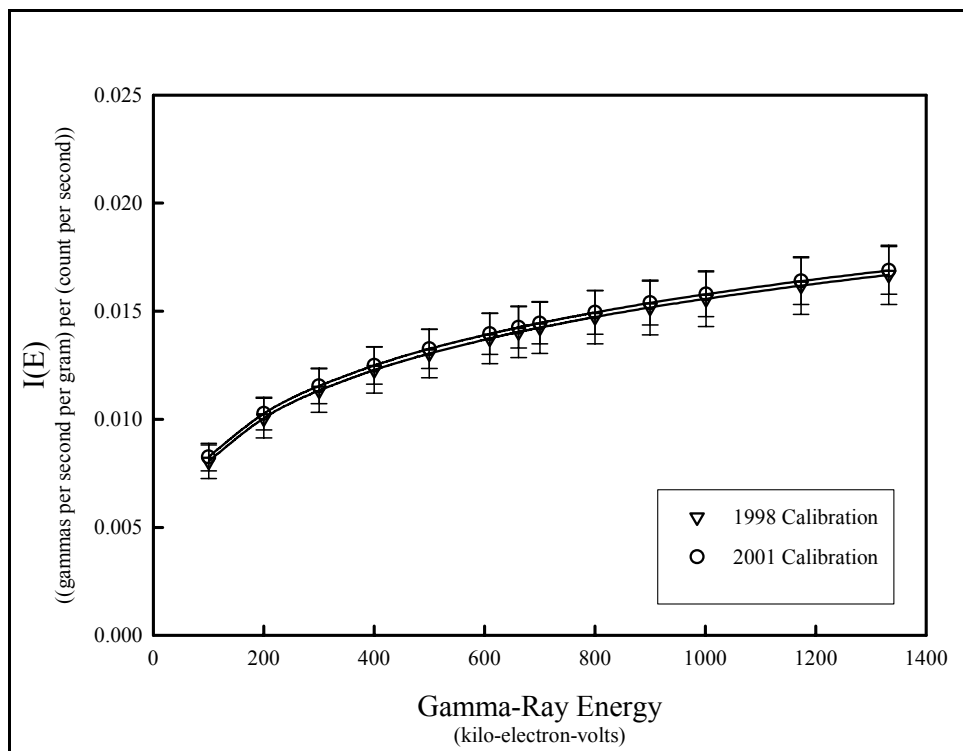


Figure 2-4. Calibration Comparisons for Gamma 2A (for the 1998 calibration, the sonde with Detector A was operated by Gamma 1)

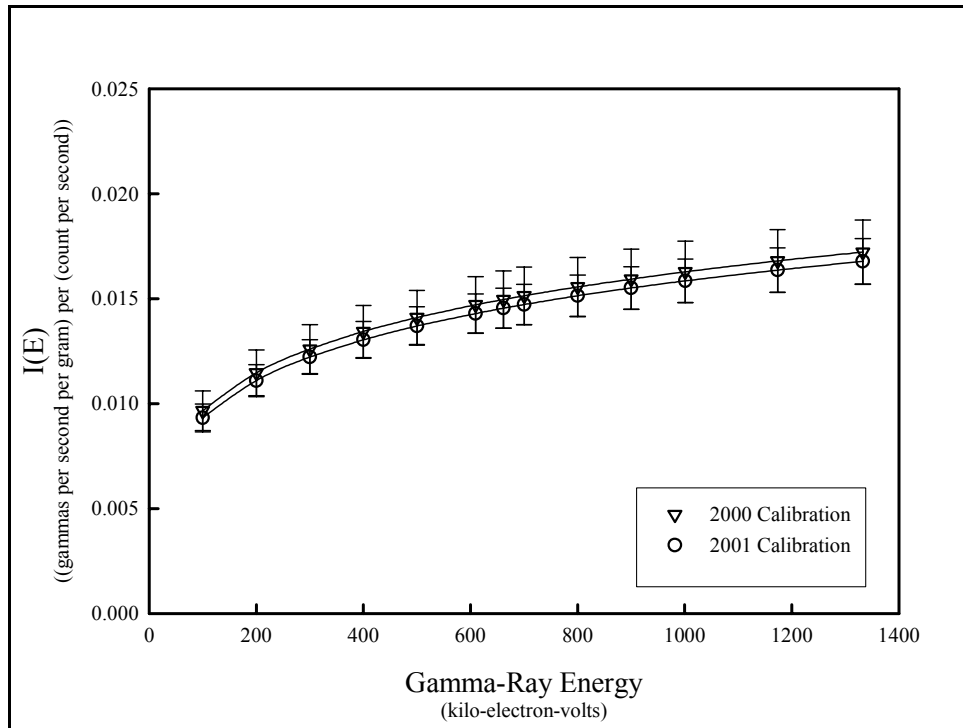


Figure 2-5. Calibration Comparisons for Gamma 2B

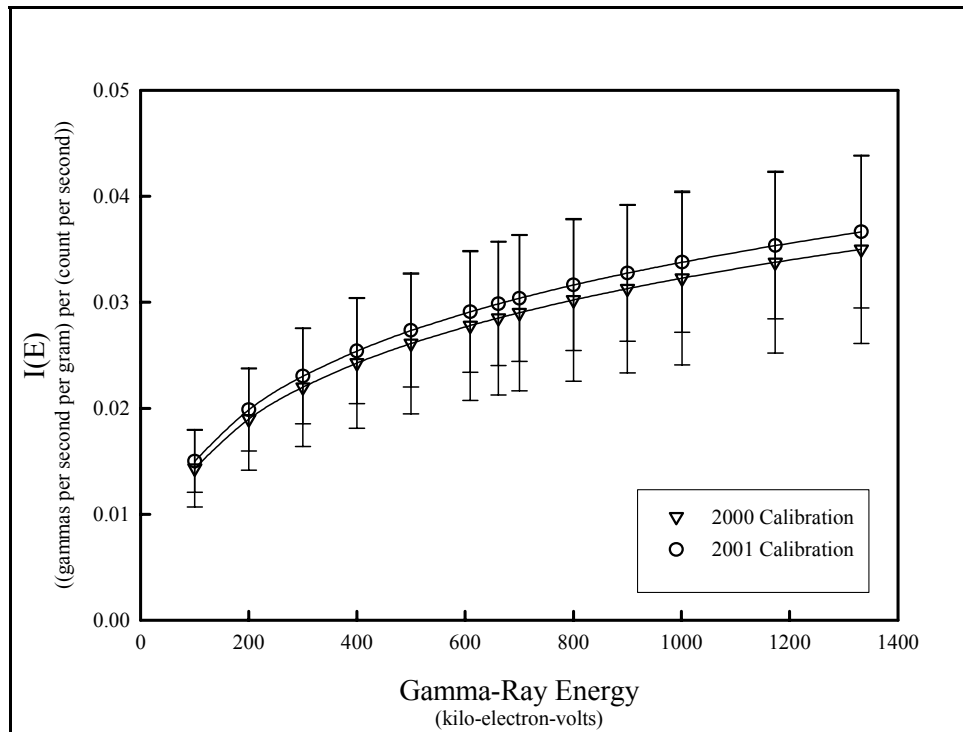


Figure 2-6. Calibration Comparisons for Gamma 1D

The data plotted in Figures 2-4, 2-5, and 2-6 indicate that the 2001 calibration functions agree, within uncertainties, with the prior calibration functions.

Table 2-9 shows calculated $I(E)$ values for some gamma rays of the most common waste constituents. For comparison, values calculated with the previous calibration constants are included.

Table 2-9. Representative $I(E)$ Values Calculated with the Previous and New Calibration Functions

Gamma-Ray Source	Gamma-Ray Energy (keV)	Gamma 2A $I(E)$ $((\gamma/s/g)/(c/s))^1$		Gamma 2B $I(E)$ $((\gamma/s/g)/(c/s))$		Gamma 1D $I(E)$ $((\gamma/s/g)/(c/s))$	
		1998	2001	2000	2001	2000	2001
^{137}Cs	661.6	0.0140 ± 0.0012	0.0142 ± 0.0010	0.0150 ± 0.0014	0.0145 ± 0.0010	0.0285 ± 0.0072	0.0298 ± 0.0058
^{60}Co	1173.2	0.0162 ± 0.0013	0.0164 ± 0.0011	0.0168 ± 0.0015	0.0164 ± 0.0011	0.0338 ± 0.0086	0.0353 ± 0.0069
^{60}Co	1332.5	0.0167 ± 0.0014	0.0169 ± 0.0011	0.0172 ± 0.0015	0.0168 ± 0.0011	0.0350 ± 0.0089	0.0366 ± 0.0072
^{152}Eu	964.0	0.0154 ± 0.0013	0.0156 ± 0.0010	0.0162 ± 0.0014	0.0157 ± 0.0010	0.0319 ± 0.0081	0.0334 ± 0.0065
^{152}Eu	1408.1	0.0169 ± 0.0014	0.0171 ± 0.0011	0.0174 ± 0.0015	0.0170 ± 0.0011	0.0335 ± 0.0090	0.0372 ± 0.0073
^{154}Eu	723.3	0.0144 ± 0.0012	0.0146 ± 0.0010	0.0152 ± 0.0014	0.0148 ± 0.0010	0.0293 ± 0.0074	0.0307 ± 0.0060
^{154}Eu	1274.8	0.0165 ± 0.0014	0.0167 ± 0.0011	0.0171 ± 0.0015	0.0166 ± 0.0011	0.0346 ± 0.0088	0.0362 ± 0.0071

¹ Gamma rays per second per gram per count per second.

2.2 Linearity Demonstration

The relationship between the recorded spectral peak intensities and the gamma-ray source intensities is linear when the counting rates are low, but the relationship becomes nonlinear at high counting rates. As described in the SGLS base calibration report (DOE 1995), the nonlinearity is a consequence of the system dead time, and corrections were developed so that the dead-time-corrected peak intensities would be linear in relation to the intensities of the associated gamma-ray sources. The dead time corrections are functions of the percent dead time T_D :

$$\text{dead time correction} = K_{DT} = \frac{1}{F + G \cdot T_D \cdot \ln(T_D) + H \cdot (T_D)^3}. \quad \text{Eq. (2-5)}$$

A dead time correction is implemented by multiplying a peak intensity, P , by the correction:

$$\text{corrected peak intensity} = P \cdot K_{DT}. \quad \text{Eq. (2-6)}$$

Section 4.1.3.1 of this report presents the equation for the uncertainty in the dead time correction.

In Equation (2-5), F , G , and H are dimensionless factors that have constant values for a particular logging vehicle. The values of F , G , and H determined by analysis of data collected during the

base calibration are displayed in Table 2-10. These values are linked to the logging vehicles, not the sondes, under the assumption that the dead time effect is influenced by the electronics, including the analog-to-digital converters, mounted in the vehicles.

Table 2-10. Constants for the Dead Time Correction

Logging Unit	$F \pm \sigma F$	$G \pm \sigma G$	$H \pm \sigma H$
Gamma 1 (HO68B3572)	1.0080 ± 0.0054	$(-4.71 \pm 0.47) \times 10^{-4}$	$(-5.73 \pm 0.21) \times 10^{-7}$
Gamma 2 (HO68B3574)	1.0322 ± 0.0022	$(-1.213 \pm 0.028) \times 10^{-3}$	$(-1.89 \pm 0.20) \times 10^{-7}$

The dead time measurements have never been repeated, but the dead time corrections are indirectly validated at each recalibration by demonstrating that the dead-time-corrected peak intensities are linearly related to the associated gamma-ray source intensities.

Data for the demonstrations were acquired by logging the calibration standards listed in Table 2-1. The spectral peak intensities for several “radium” gamma rays were corrected for dead time, then plotted in relation to ^{226}Ra concentration. ^{226}Ra concentrations ranged from 1.16 picocuries per gram to 902 pCi/g, and the system dead times ranged from less than 1 percent to slightly higher than 70 percent.

All of the data conformed to the expected linear relationships. Some examples are presented in peak-intensity-versus-source-concentration plots in Figures 2-7 through 2-11.

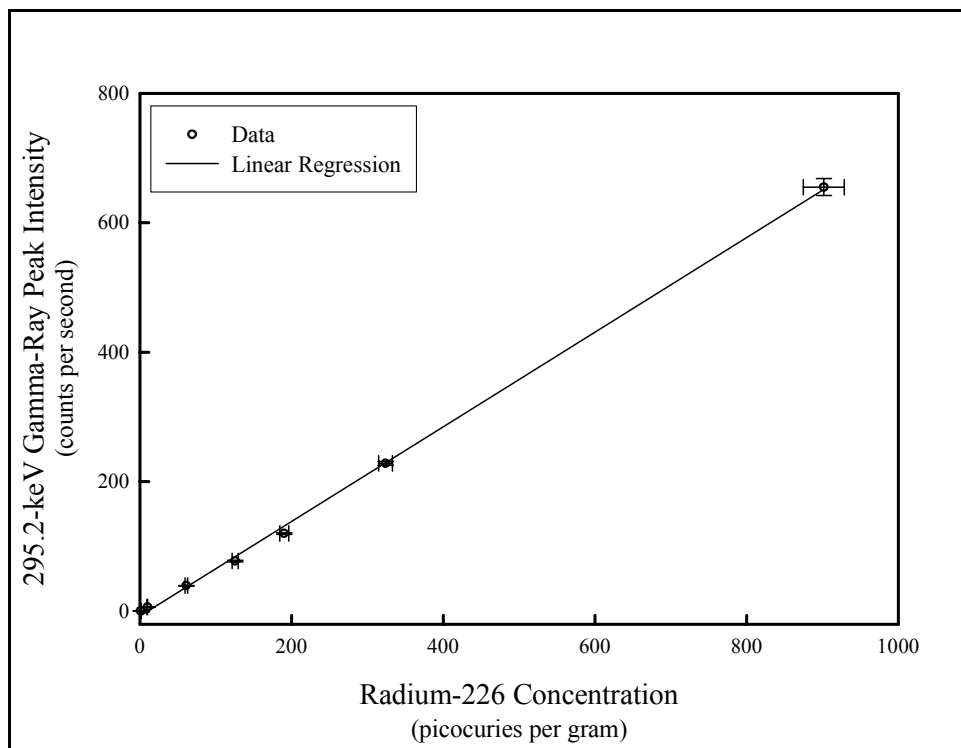


Figure 2-7. Linearity Demonstration for Gamma 2A and the 295.2-keV

Gamma-Ray Peak

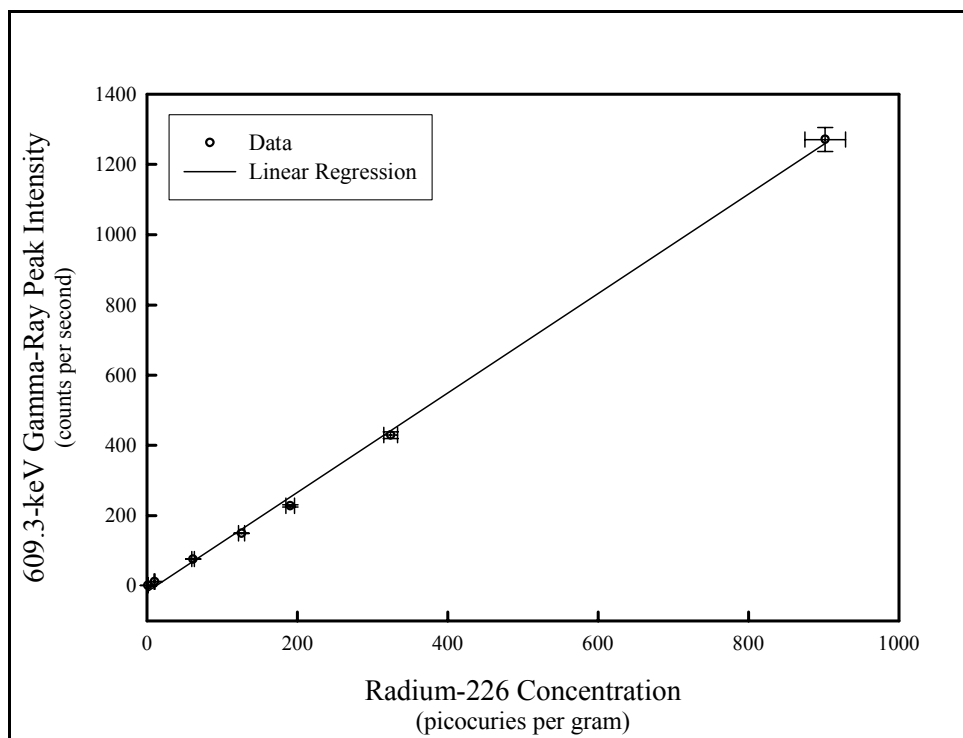


Figure 2-8. Linearity Demonstration for Gamma 2A and the 609.3-keV Gamma-Ray Peak

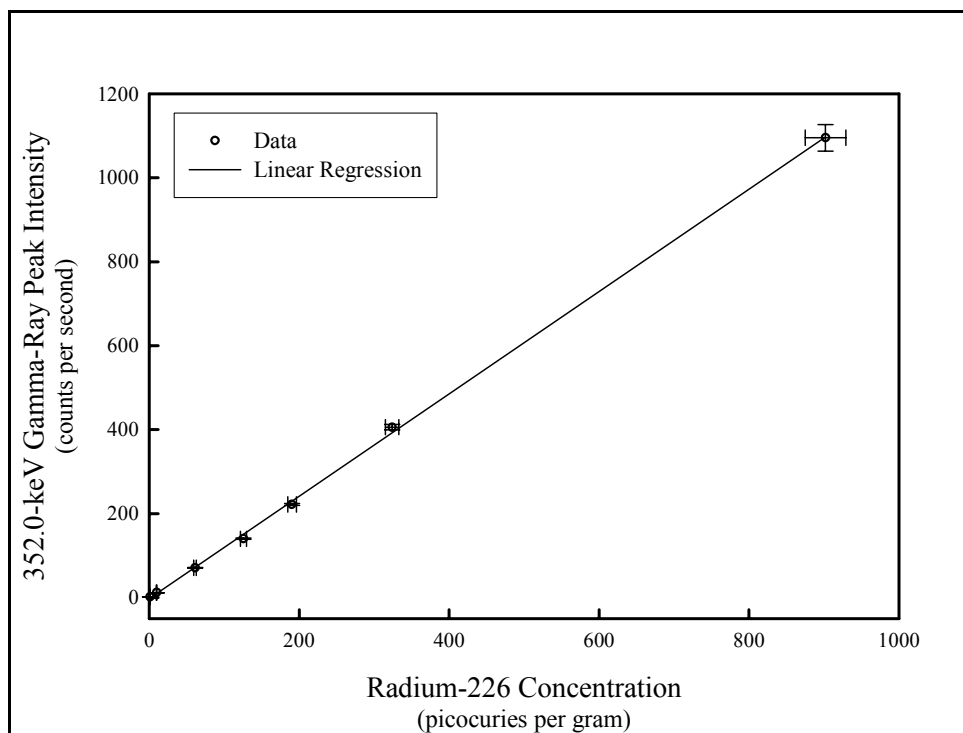


Figure 2-9. Linearity Demonstration for Gamma 2B and the 352.0-keV

Gamma-Ray Peak

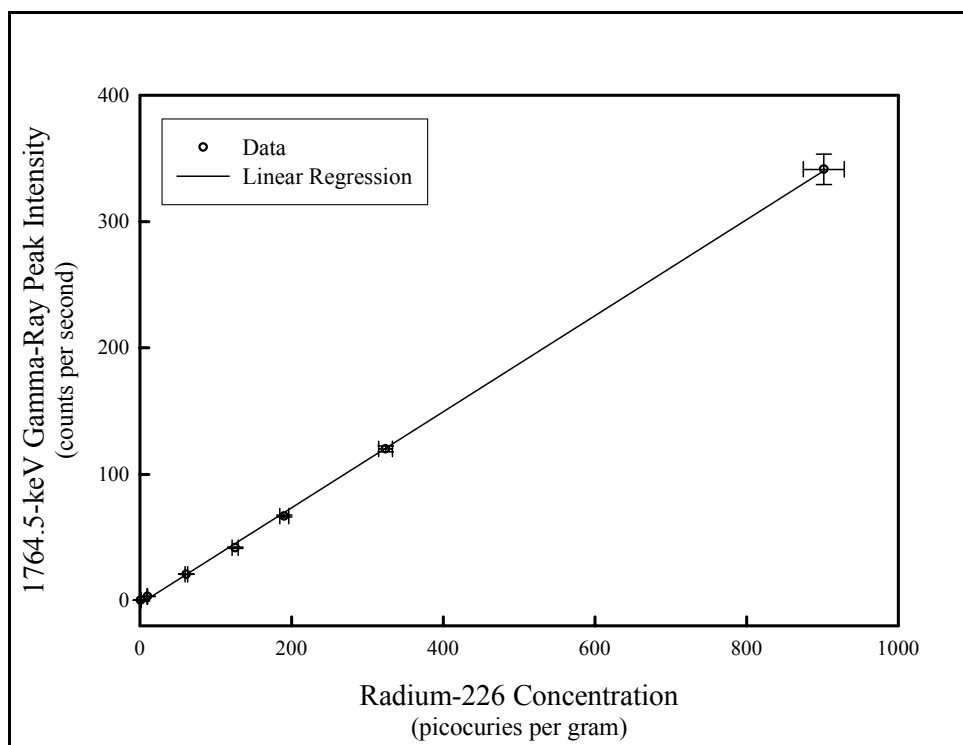


Figure 2-10. Linearity Demonstration for Gamma 2B and the 1764.5-keV Gamma-Ray Peak

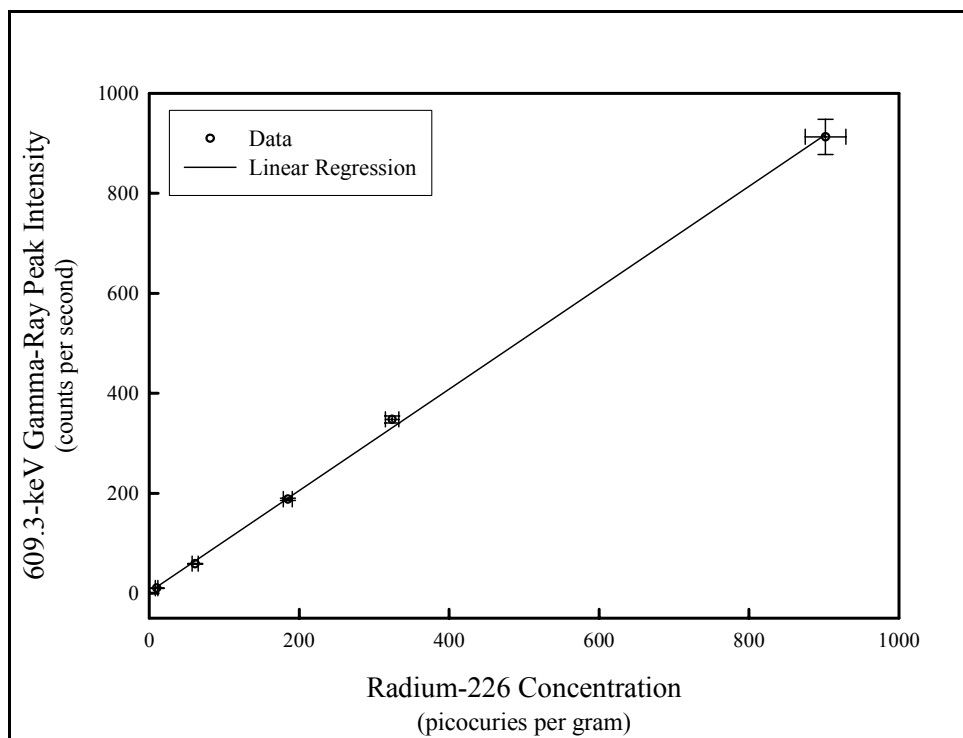


Figure 2-11. Linearity Demonstration for Gamma 1D and the 609.3-keV

2.3 Revised Field Verification Criteria

When an SGLS is engaged in routine operations, field verification spectra are recorded at the beginning and end of each day to confirm that the logging system is operating properly. These spectra are acquired with an *Amersham KUTh Field Verifier* (Amersham part number 188074) potassium-uranium-thorium source mounted on the sonde. Each spectrum has three prominent full energy peaks associated with the 609.3-keV gamma ray of ^{214}Bi (^{238}U decay product), the 1460.8-keV gamma ray of ^{40}K , and the 2614.5-keV gamma ray of ^{208}Tl (^{232}Th decay product). Logging system performance evaluation is based on the intensities and full widths at half maxima (FWHM) of these three peaks. Consistent with conventional control chart practices (Taylor 1987), the intensities and FWHM are compared to acceptance tolerances derived from statistical analyses of peak intensities and FWHM from many previously recorded verification spectra.

Until recently, acceptance tolerances were formulated in terms of warning and control limits for peak intensities and FWHM for the spectral peaks associated with the three gamma rays. To derive the limits, means and standard deviations (σ) for intensity and FWHM for the three gamma-ray peaks were calculated using a large number of verification spectra. Warning limits were established as the 2-sigma (2σ) deviations from the mean values, and control limits were established as the 3-sigma (3σ) deviations:

$$\begin{aligned}\text{upper control limit} &= \text{mean} + 3\sigma \\ \text{upper warning limit} &= \text{mean} + 2\sigma \\ \text{lower warning limit} &= \text{mean} - 2\sigma \\ \text{lower control limit} &= \text{mean} - 3\sigma.\end{aligned}$$

The tolerances were used as follows. After a field verification spectrum was recorded, intensities and FWHM for the three gamma-ray peaks were compared to the appropriate tolerances. For a particular intensity or FWHM, 95 percent of readings should have fallen between the two warning limits, so the occurrence of an intensity or FWHM outside of this range was taken as an indication of a possible logging system malfunction. Essentially all of the readings should have fallen between the lower and upper control limits; therefore, a logging system malfunction was considered likely if a reading outside of the control limits occurred.

Near the end of 2001, the verification methods were modified to account for systematic daily drifts in SGLS efficiency that were observed during 2001. These drifts were confirmed for all of the systems by separating the field verification spectra into two sets: those acquired prior to logging runs (pre-survey spectra) and those acquired after logging runs (post-survey spectra), and statistically analyzing the two sets. The peak intensities in the post-survey set were consistently lower than the analogous intensities from the pre-survey set. The reason for this drift is unknown, but examinations of field verification spectra acquired over the years indicate that the drift has been a long-term feature of the logging systems.

The warning and control limits had been previously derived by analyzing a large group of field verification spectra, without separating the pre-survey spectra from the post-survey spectra. The acceptance limits were recently modified, as follows, to account for daily efficiency drift. For the spectral peaks associated with the three gamma rays (609.3 keV, 1460.8 keV, and 2614.5 keV), means and standard deviations of the intensities and FWHM were calculated using verification spectra collected during calibration. Each tolerance range was then defined as follows:

upper control limit = mean + 3σ

lower control limit = mean - 3σ

calculated from the post-survey data.

The use of warning limits has been discontinued.

For pre-run verification criteria, both peak intensity and FWHM are compared to the control limits. If a peak intensity or FWHM from a verification spectrum falls outside of the control limit range, the system fails the field verification test and the cause of the failure must be determined and corrected before additional logging is performed. For post-run verification spectra, FWHM values are compared to the control limits, but post-run peak intensity values are compared to corresponding pre-run values. Comparison of pre-run and post-run verification spectra indicates that the change in peak intensity over the course of a logging day is generally on the order of 6 to 8 percent. Because the most important concern is the extent of drift over the course of the logging run(s), post-run peak intensities are judged to be acceptable if they fall within 10 percent of the corresponding value measured at the beginning of the logging day.

Pre-run verification spectra are typically processed and evaluated by the logging engineer while logging is underway. In addition, the logging engineer monitors spectra as they are collected during the log run, making fine gain adjustments as necessary to maintain consistent peak position. A catastrophic logging system malfunction would thus be noticed immediately. Post-run verification spectra are not processed and evaluated until the next day, or possibly not until the log data are processed. The delay is inconsequential; the post-run data have no immediate use in the field because the log has already been recorded. If a system malfunction has occurred, it will be evident in the pre-run verification measurement collected on the next day. The primary value of the post-run verification data is in assessing the quality of a log run and determining if the borehole should be re-logged.

Widespread ^{137}Cs surface contamination at Hanford produces variable background radiation which, together with changes in ambient conditions, may cause subtle variations in verification readings. Hence, failure to meet verification criteria is not a positive indication of system malfunction. If a verification failure occurs, the technical lead is notified and the verification and log spectra are examined to assess the problem. Verification results outside the control limits may be conditionally accepted if the analyst and technical lead are able to rule out a system malfunction. If the possibility of a system malfunction cannot be dismissed, the logging system will be checked for proper functioning. In some cases it may be necessary to re-log all or part of

a borehole. Verification failures are noted in the log data reports, along with brief comments on the reliability of the log data.

Table 2-11. Gamma 2A Field Verification Criteria

	609.3 keV		1460.8 keV		2614.5 keV	
	Peak Intensity (c/s)	Peak FWHM (keV)	Peak Intensity (c/s)	Peak FWHM (keV)	Peak Intensity (c/s)	Peak FWHM (keV)
Upper Control Limit	9.833	2.97	10.541	3.19	2.354	3.61
Lower Control Limit	7.731	1.55	9.209	1.93	1.988	2.37

Table 2-12. Gamma 2B Field Verification Criteria

	609.3 keV		1460.8 keV		2614.5 keV	
	Peak Intensity (c/s)	Peak FWHM (keV)	Peak Intensity (c/s)	Peak FWHM (keV)	Peak Intensity (c/s)	Peak FWHM (keV)
Upper Control Limit	10.477	3.26	12.102	3.36	2.828	3.63
Lower Control Limit	6.426	1.03	7.965	1.59	1.660	2.27

Table 2-13. Gamma 1D Field Verification Criteria

	609.3 keV		1460.8 keV		2614.5 keV	
	Peak Intensity (c/s)	Peak FWHM (keV)	Peak Intensity (c/s)	Peak FWHM (keV)	Peak Intensity (c/s)	Peak FWHM (keV)
Upper Control Limit	8.886	2.71	9.698	2.98	2.139	3.63
Lower Control Limit	6.481	1.54	7.105	2.05	1.514	2.50

3.0 Neutron-Neutron System Calibration

3.1 Operation

The neutron-neutron sonde has an Am-Be neutron source and a boron trifluoride neutron detector (Detector F, serial number H380932510). During logging, neutrons from the source enter the medium surrounding the sonde and lose kinetic energy through elastic collisions with hydrogen. After several such collisions, a neutron typically loses most of its kinetic energy and attains thermal equilibrium with its surroundings. The distribution of such thermal neutrons depends on the density of hydrogen in the medium. Because hydrogen normally occurs in water, the volume density of water in the logged medium influences the extent of the thermal neutron “cloud” around the sonde, which affects the thermal neutron flux at the detector. The boron trifluoride detector is sensitive primarily to thermal neutrons.

The source-to-detector spacing of the sonde, approximately an inch, is much smaller than the spacings of around 22 to 26 in. that are typical for petroleum industry neutron-neutron sondes. In fact, a neutron source and thermal neutron detector in a short-spaced configuration is often called a “moisture gauge” instead of a neutron logging device. Pros and cons of long and short spacings are discussed by Hearst and Carlson (1994). The tradeoff of significance to Hanford logging is that the larger volume of interrogation provided by the long spacing is sacrificed for the superior vertical spatial resolution provided by the short spacing. Neutron-neutron devices with short source-to-detector spacings have the property that the count rate increases as the moisture content of the logged medium increases.

The logging system calibration relates the count rate to the volume fraction of water (VF) in the medium surrounding the borehole.

3.2 Calibration Standards

Six calibration standards, described by Engelman et al. (1995), reside at the Hanford Site calibration center near the main entrance to the 200 West Area. The standards are large cylindrical tanks filled with unconsolidated mixtures of sand and hydrated alumina ($\text{Al}_2\text{O}_3 \cdot 3\text{H}_2\text{O}$); each standard has a particular hydrated alumina content, and thus, a particular VF. Test holes in the standards are cased with 6-in.-diameter steel casing or 8-in.-diameter steel casing. The properties are tabulated in Table 3-1 (from Engelman et al. 1995).

Table 3-1. Properties of the Calibration Standards

Standard Name	Casing Inside Diameter (in.)	Volume Fraction of Water	Specific Gravity
F	6 ¹	0.050	1.76
E	6	0.117	1.74
G	6	0.198	1.70
A	8 ²	0.050	1.76

Standard Name	Casing Inside Diameter (in.)	Volume Fraction of Water	Specific Gravity
C	8	0.119	1.76
B	8	0.197	1.70

¹ The 6-in. casing has a 0.28-in.-thick wall.

² The 8-in. casing has a 0.32-in.-thick wall.

Engelman et al. (1995) established the VF values using the masses of sand and hydrated alumina that were placed in the standards. Uncertainties for the VF values were not reported. Samples of the calibration standard materials were collected when the standards were constructed, but the samples have not been analyzed to corroborate the VF values in Table 3-1.

Sand usually contains non-trivial amounts of water, especially if stored outside. During the 1970s and early 1980s, when sand was used to construct DOE-GJO calibration standards, engineers attempted to track or control the water contents of the finished products by using kiln-dried sand or by measuring the water content of the sand immediately prior to incorporation of the sand in the calibration standard concrete mix (Koizumi 1981). Such methods were apparently not used for the VF standards; therefore, the VF values might actually be slightly higher than those reported.

It should also be noted that the calibration standards were constructed in 1995 and initially housed in the Neil F. Lampson facility in Pasco, Washington. The models were transported to their present location near the 200 West Area on the Hanford Site sometime around September 1999. Because the material in the standards is unconsolidated, the relocation may have subjected the material to compaction, differential settling, or other processes that could have affected the properties in Table 3-1.

3.3 Calibration Data

During 2001, the neutron-neutron system was calibrated twice. The first calibration data were collected in May 2001 with the sonde operated by the logging unit Gamma 2. For each set of measurements, a centralizer was mounted on the sonde to hold it centered in the test hole, then the sonde was lowered into a standard until the center of the source-detector was approximately at the (vertical) center of the standard. Six pulse height spectra were acquired from each standard with the position of the sonde fixed; the acquisition time was 100 seconds (live time) per spectrum.

To simulate measurements in a zero-moisture environment, a set of six spectra was acquired with the sonde suspended in air with the detector about 8 in. above the ground.

The second set of calibration data was acquired in November 2001 with Gamma 2F. The measurements were identical to the May 2001 measurements, except for the following:

- For calibration, the counting times were 60 seconds per spectrum, instead of 100 seconds

per spectrum.

- The air measurements were not repeated.
- Data were collected by logging the F standard with the sonde enclosed in a plastic sleeve of the type that is typically used at Hanford to minimize contamination of the sonde. These data were acquired to determine the effect (if any) of the plastic sleeve on measurements.
- Data were collected by logging the F standard with a section of 4.0-in.-diameter, 0.25-in.-thick steel casing placed in the test hole. The casing section was located inside of the 0.28-in.-thick steel casing that is permanently installed in the F standard.

All of the calibration spectra were analyzed with the spectrum analysis program *PCMCA/WIN* (Version 6.3.1, release 13, Aptec Engineering Limited, North Tonawanda, New York). Analysis consisted simply of determining the gross count rate for each spectrum. No corrections were applied to the count rates. The weighted average count rates are displayed in Table 3-2. In all cases, the measurement precision was good, as indicated by the small count rate uncertainties.

Table 3-2. Calibration Count Rate Data

Standard Name	Casing Diameter (in.)	Count Rates (May) (c/s)	Count Rates (Nov.) (c/s)
F	6	185.2 ± 1.1	187.3 ± 1.4
E	6	271.4 ± 1.3	276.3 ± 1.8
G	6	342.1 ± 1.5	349.8 ± 2.0
A	8	145.9 ± 1.0	148.2 ± 1.3
C	8	204.4 ± 1.2	208.2 ± 1.5
B	8	248.1 ± 1.3	253.9 ± 1.7

The system dead time effect could not be measured, but the maximum observed dead time was only 1.3 percent, and dead time effects were almost certainly negligible.

3.4 Calibration Results

Because the test holes in the calibration standards have two casing sizes, two distinct calibrations were derived. One calibration applies to data acquired by logging a borehole with a 6-in. steel casing (0.28-in. wall thickness); the other is for data from boreholes with 8-in. steel casing (0.32-in. wall thickness). Most of the existing Hanford boreholes have either 6-in. or 8-in. steel casing.

The count rate and VF data were analyzed with the *TableCurve* (Version 1.11, Jandel Scientific, San Rafael, California) curve fitting program. The curve fitting was guided by a calibration function,

$$VF = A \cdot (\text{count rate})^\alpha, \quad \text{Eq. (3-1)}$$

which was previously established for the sonde by Dr. R.R. Randall of Three Rivers Scientific. Randall's calibration is documented by a "Certificate of Calibration for RLSM3.1," dated January 30, 1997 ("RLSM3.1" is Three Rivers Scientific's name for the sonde).

The function that was actually used in the curve fitting was

$$\ln(VF) = A + B \cdot \ln(R), \quad \text{Eq. (3-2)}$$

which is one of the functions in the *TableCurve* repertoire. R is the count rate, and A and B are constants. An equation that is equivalent to Equation (3-2) is

$$VF = e^A \cdot e^{B \cdot \ln(R)} = e^A \cdot R^B, \quad \text{Eq. (3-3)}$$

which has the same form as the function used by Randall (Equation (3-1)). Equation (3-3) is the calibration equation, and A and B are the calibration constants.

Equation (3-3) fits the calibration data very well, as indicated by the plots in Figures 3-1 and 3-2. Figure 3-1 shows the November 2001 data points and the fitted calibration function for the 6-in. casing, and Figure 3-2 shows the November 2001 data points and the fitted calibration function for the 8-in. casing.

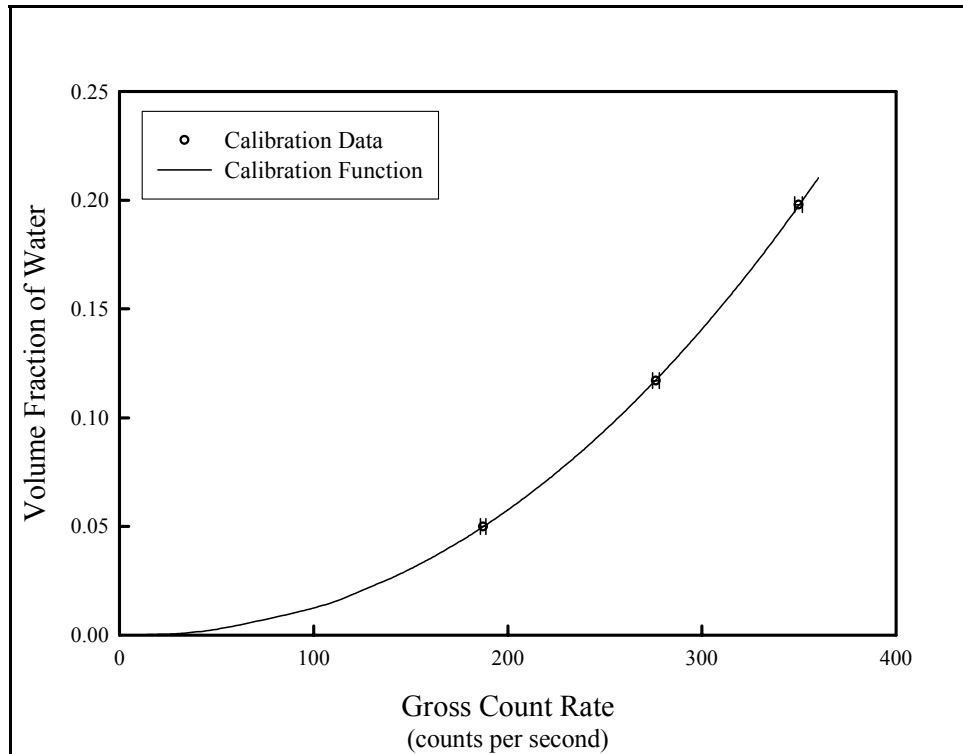


Figure 3-1. November 2001 Calibration Curve for the 6-in. Casing

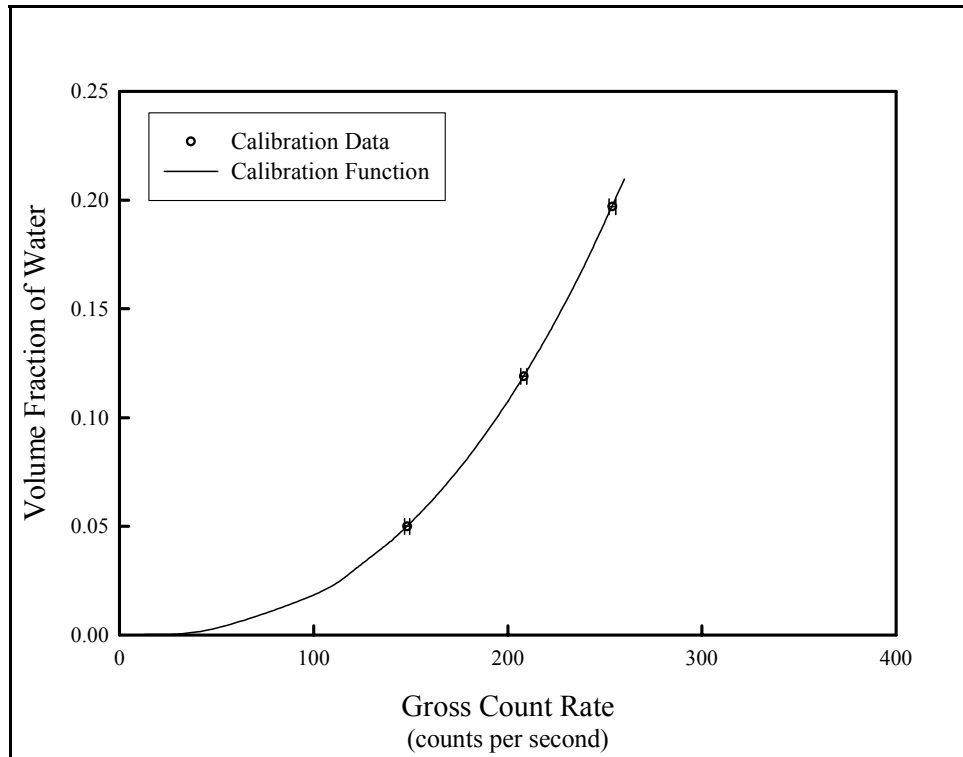


Figure 3-2. November 2001 Calibration Curve for the 8-in. Casing

In Figures 3-1 and 3-2 the error bars on the calibration data points are almost invisible because the lengths of the error bars are approximately equal to the radii of the symbols.

The calibration constant values inferred from the curve fitting are as follows:

May 2001 Calibration

6-in. casing

$$A = -14.77 \pm 1.14$$

$$B = 2.253 \pm 0.198$$

8-in. casing

$$A = -15.902 \pm 0.438$$

$$B = 2.5894 \pm 0.0807$$

Effective period: May 3, 2001 to November 13, 2001.

November 2001 Calibration

6-in. casing

$$A = -14.52 \pm 0.58$$

$$B = 2.203 \pm 0.087$$

8-in. casing

$$A = -15.720 \pm 0.073$$

$$B = 2.546 \pm 0.012$$

Effective period: November 14, 2001 to the date of the next recalibration.

The measurements acquired in May 2001 with the sonde suspended in air yielded a weighted average count rate of 4.16 ± 0.17 counts per second. This count rate is proposed to correspond closely to $VF = 0$ because the volume fraction of water in air was too low to thermalize many neutrons near the detector, where such thermal neutrons would have a non-negligible probability of entering the detector. In Figures 3-3 and 3-4, small squares labeled “Air Point” mark the air measurement point ($R = 4.16$, $VF = 0$) in relation to the May 2001 calibration results. *The air point was not used to establish the calibration constants, but the point lies on both calibration curves.* That is, if the count rate of 4.16 counts per second is substituted for R in the two calibration equations, the calculated VF values are close to zero. (For $R = 4.16$ counts per second, the VF values are 9.6×10^{-6} for the 6-in. casing, and 5.0×10^{-6} for the 8-in. casing.) This is a critical finding because it suggests that the calibration curves can be extrapolated to values of VF below the range spanned by the calibration standards. This would justify the use of the calibration to determine very low values of VF that might be encountered in the Hanford vadose zone.

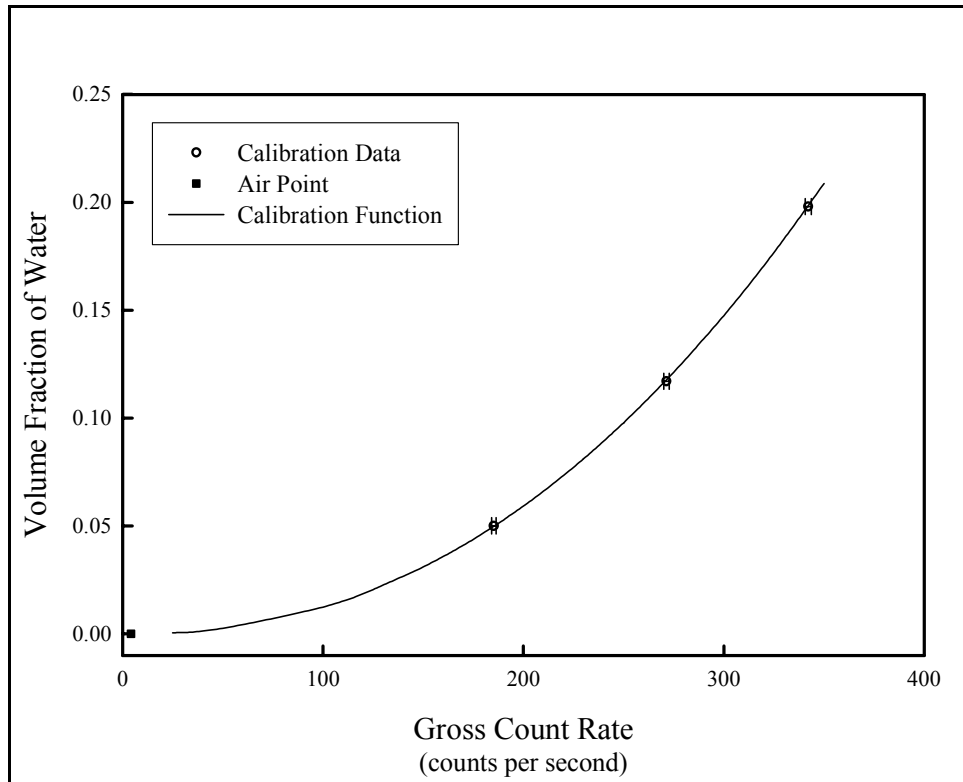


Figure 3-3. May 2001 Calibration Curve for the 6-in. Casing

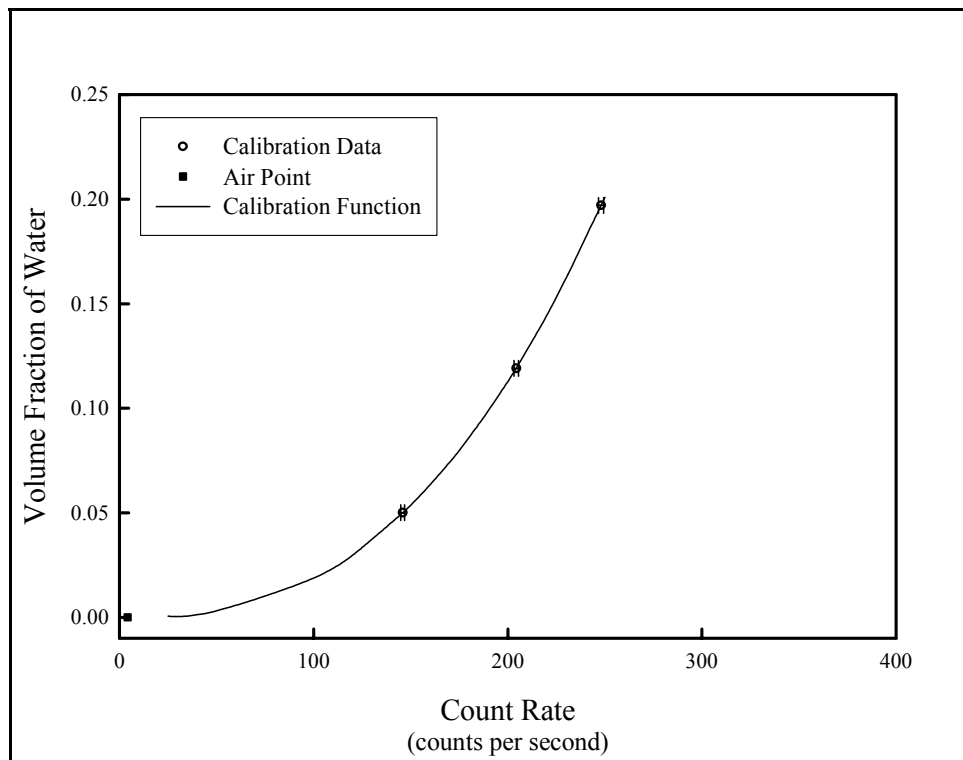


Figure 3-4. May 2001 Calibration Curve for the 8-in. Casing

3.5 Comparisons to Earlier Calibrations

Users of neutron-neutron log data may be interested in comparing the November 2001 calibrations with previous calibrations. The system was calibrated in May 2001, and the same sonde (operated by a different logging system) was calibrated earlier, as documented by Dr. R.R. Randall in a “Certificate of Calibration for RLSM3.1” dated January 30, 1997. For these comparisons, the calibration constants presented in this report and the Randall calibrations were used to calculate VF values for the 6-in. casing and the count rates 100, 125, 150, 175, ..., 350 counts per second, and the 8-in. casing and the count rates 100, 125, 150, 175, ..., 250 counts per second. The results are displayed in Figures 3-5 and 3-6.

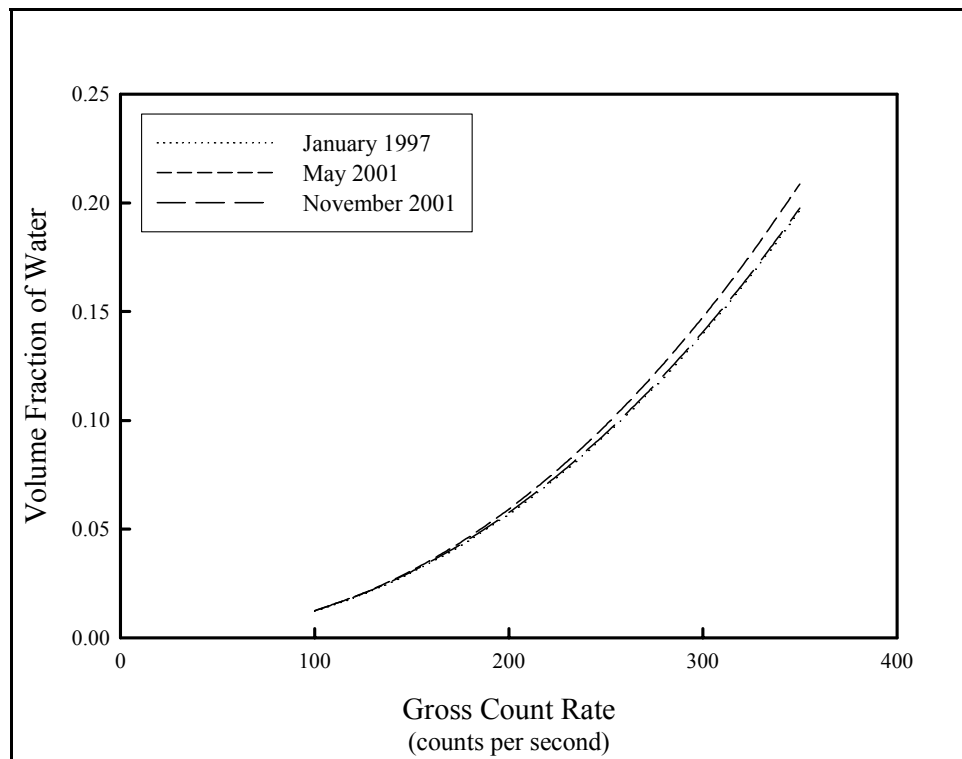


Figure 3-5. The 6-in. Casing Calibration Functions

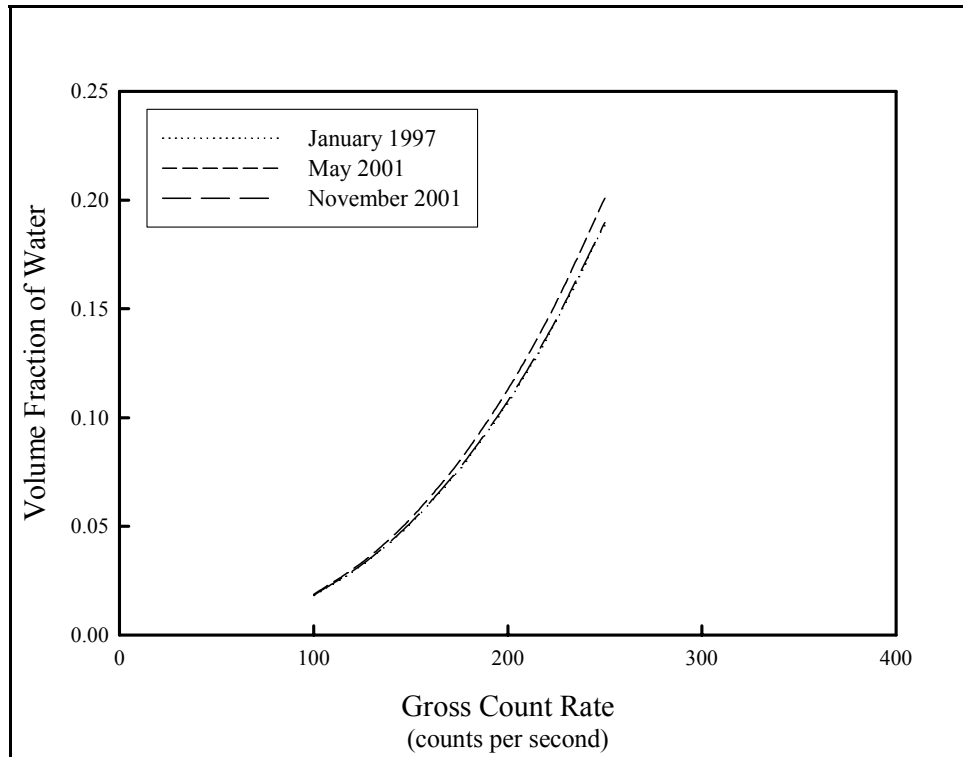


Figure 3-6. The 8-in. Casing Calibration Functions

The plots in Figures 3-5 and 3-6 indicate that the January 1997 and November 2001 calibration functions are essentially identical. These plots and the entries in Table 3-2 indicate that the efficiency of the neutron detector was apparently slightly lower when the May 2001 calibration data were acquired. One favorable feature of the calibrations is that the curves for a given casing converge as the count rate decreases. This indicates that for either casing size, the count-rate-to-VF conversions embodied in the three calibrations are essentially identical at the low VF values that should be typical of the Hanford vadose zone.

3.6 Effect of a Plastic Sleeve Covering the Sonde

During the May 2001 measurements, six spectra were acquired, at 100 seconds per spectrum, by logging the F standard with a plastic sleeve covering the sonde. The sleeve was the type normally used at Hanford to prevent sonde contamination during logging. The weighted average gross count rate recorded without the sleeve was 185.2 ± 1.1 counts per second, while the rate recorded with the sleeve was 185.0 ± 1.1 counts per second. The ratio of the no-sleeve rate to the rate with the sleeve is 1.0011 ± 0.0085 . The ratio is essentially equal to one, meaning that the effect of the sleeve is negligible.

3.7 Effect of a 4.0-in.-Diameter, 0.25-in.-Thick Steel Casing Inside of a 6-in. Casing

During the May 2001 calibration measurements, data were also acquired for a limited assessment

of steel casing effect. Six spectra were recorded, at 100 seconds per spectrum, by logging the F standard with a section of 4.0-in.-diameter, 0.25-in.-thick steel casing placed in the test hole. The casing section was located inside of the 0.28-in.-thick steel casing that is permanently installed in the F standard. The weighted average gross count rate was 150.0 ± 1.0 counts per second. The ratio of the count rate with the casing section to the rate without the casing section was 0.810 ± 0.007 , indicating that the casing section reduced the gross count rate by about 19 percent. The inverse of this ratio, 1.235 ± 0.011 , can be regarded as a correction for the particular casing configuration. That is, the gross count rate recorded in a borehole with a 4.0-in.-diameter, 0.25-in.-thick casing inside of a 6-in.-diameter, 0.28-in.-thick steel casing can be multiplied by 1.235 to determine the count rate that would have been recorded in the absence of the 0.25-in.-thick casing. It should be noted that the neutron-neutron response was probably sensitive to the air gap between the 6.0-in. and 4.0-in. casings; therefore, a calculated VF value may not be accurate if this correction is applied to a measurement involving an inner casing with a thickness of 0.25 in., but a diameter different from 4.0 in. This correction also does not account for the presence of grout in the annular space between the two casings.

3.8 Limitations

Within a calibration standard, the sonde is surrounded by a large, homogeneous mass of material with a uniform concentration of water. The calibration results are specific to this measurement condition. Thus, accurate VF values may not be attained if the sonde encounters materials in a different array, for example, layers of thin zones with varying VF values.

The calibration curves plotted in Figures 3-3 and 3-4 show that for each VF value the neutron count rate for the 6-in. test hole was significantly different from the count rate for the 8-in. test hole. The sensitivity of the neutron responses to the casing parameters shows that the calibrations are definitely casing-specific. Accurate VF values cannot be expected unless a borehole casing has a diameter and thickness that nearly coincide with the diameter and thickness of the 6-in. or the 8-in. casing in the calibration standards.

The calibration standard materials have slight variations in bulk density, as indicated by Table 3-1, but perturbations on the calibration measurements caused by these variations were most likely negligible. Because the calibration standard materials have nearly identical bulk densities, the effects of bulk density changes could not be measured. The calibration standard materials were formulated to have bulk density values close to typical values for Hanford vadose zone deposits (Engelman et al. 1995) so that log data would not require bulk density corrections. Consequently, bulk density effects were ignored in the analysis of calibration data, and no correction is applied to offset the bulk density effect when the calibration is used to calculate VF values. The bulk density effect is strongly specific to the sonde design, but the magnitude of the effect can be estimated from moisture gauge measurements by P. Couchat cited in an International Atomic Energy Agency (IAEA) report (IAEA 1970). For the moisture gauge used by Couchat, the change in VF per change in bulk density was approximately 0.1 (or 10 percent) per gram per cubic centimeter.

A number of common elements have isotopes with large thermal neutron absorption cross sections. If a medium being logged contains such elements, even in minute concentrations, the thermal neutron absorption rates will be high, the thermal neutron fluxes will be low, and the calculated VF values will be spuriously low, relative to a medium lacking such elements. VF calculations thus rely on the assumption that the macroscopic thermal neutron absorption cross sections of the logged media are not significantly different from the corresponding cross sections for the materials in the calibration standards.

Inherent in the sonde's short source-to-detector spacing is a small volume of interrogation. The measurement is dominated by the material that is essentially adjacent to the sonde. Thus, a measurement of the formation VF is unattainable if the borehole casing is grouted, or if the borehole is filled with water.

Equation (3-3) (the calibration equation) is not accompanied by an equation for the calculation of the *uncertainty* in VF. The reason is that the conventional equations for propagation of uncertainties give huge relative uncertainties for the calculated VF values. When applied to Equation (3-3), the propagation of uncertainties method yields the following expression for the uncertainty in VF:

$$\sigma VF = \sqrt{\left(\frac{\partial(VF)}{\partial A} \cdot \sigma A\right)^2 + \left(\frac{\partial(VF)}{\partial R} \cdot \sigma R\right)^2 + \left(\frac{\partial(VF)}{\partial B} \cdot \sigma B\right)^2}. \quad \text{Eq. (3-4)}$$

The partial derivatives can be calculated and substituted into Equation (3-4). The result is

$$\sigma VF = (VF) \cdot \sqrt{(\sigma A)^2 + \frac{4 \cdot B^2}{R} + (\ln(R) \cdot \sigma B)^2}. \quad \text{Eq. (3-5)}$$

Table 3-3 presents some examples of σVF values calculated using the May 2001 calibration for the 6-in. casing. The relative uncertainties $[(\sigma VF)/(VF)]$ exceed 150 percent.

Table 3-3. Examples of Calculated VF and Uncertainty Values

Count Rate (c/s)	VF Calculated with Equation (3-3)	Uncertainty in VF Calculated with Equation (3-5)
50	0.0026	0.0039
100	0.012	0.019
200	0.059	0.092
300	0.15	0.24
350	0.21	0.34

The relative uncertainties are apparently large because the calibration constants A and B in Equation (3-3) appear as exponents. Thus, the relatively small uncertainties in A and B produce large uncertainties in VF. This problem requires further investigation.

4.0 Summary

4.1 Spectral Gamma Logging System (SGLS)

This report describes four new results: revised calibration constants, the revised field verification criteria, and revised methods for calculating casing corrections and water-filled borehole corrections.

The dead time corrections described in the base calibration report (DOE 1995) were not revised, but were indirectly confirmed by showing that dead-time-corrected peak intensities are linear in relation to the corresponding gamma-ray source intensities.

Environmental corrections, such as corrections for casing, tungsten shield, and water-filled boreholes, are assumed unchanged; therefore, measurements to reconfirm such corrections were not conducted. However, the methods by which the casing and water corrections are calculated were revised, as described in Appendix A and Appendix B.

For reference purposes, all of the results, those revised and those unchanged, are presented in this summary.

Symbols have been assigned to various functions and quantities. Table 4-1 lists these symbols, the associated functions or quantities, and the customary units.

Table 4-1. Symbols, Functions and Quantities, and Customary Units

Symbols	Functions, Quantities, and Units
$I(E)$	Calibration function [(gamma rays per second per gram) per (count per second)]
E	Gamma-ray energy [kilo-electron-volts]
P	Spectral peak intensity [counts per second]
R	Count rate for the total spectrum or a portion of the spectrum [counts per second]
K_{XX}	Correction; XX = additional description, e.g., DT for dead time
S_I	Gamma-ray source intensity [gamma rays per second per gram of sample material]
Y	Gamma-ray yield [gamma rays per decay]
S_C	Gamma-ray source concentration [picocuries per gram of sample material]
A, B, C	Calibration constants
F, G, H	Dead time correction constants
J, L, M	Tungsten shield correction constants
Q_A, Q_B, Q_C	Casing correction factors for general casing thickness ¹
T	Casing wall thickness [inches]
W_A, W_B, W_C	Water-filled borehole correction factors for general borehole diameters ²
D	Borehole diameter [inches]

¹ Koizumi (2000).

² Koizumi (2000).

4.1.1 Calibration Functions

The calibration function

$$I(E) = (A + B \cdot \ln(E))^2 \quad \text{Eq. (4-1)}$$

was established by the base calibration (DOE 1995). The revised values for the calibration constants, A and B , are as follows:

Gamma 2A

(detector serial number 34TP20893A)

$$A = 0.0213 \pm 0.0029$$

$$B = 0.01510 \pm 0.00043$$

effective period: November 28, 2001 to the date of the next recalibration

Gamma 2B

(detector serial number 36TP21095A)

$$A = 0.0378 \pm 0.0028$$

$$B = 0.01275 \pm 0.00043$$

effective period: November 12, 2001 to the date of the next recalibration

Gamma 1D

(detector serial number 34TP11019B)

$$A = 0.0266 \pm 0.0026$$

$$B = 0.01622 \pm 0.00039$$

effective period: July 17, 2001 to the date of the next recalibration

The units of $I(E)$ will be (gamma rays per second per gram) per (count per second) when the gamma-ray energy E is expressed in kilo-electron-volts.

The uncertainty of $I(E)$ is

$$\sigma I(E) = 2 \cdot \sqrt{I(E)} \cdot \sqrt{(\sigma A)^2 + (\ln(E) \cdot \sigma B)^2} . \quad \text{Eq. (4-2)}$$

If the intensity of a spectral full energy peak (corrected for dead time, casing, and other applicable effects) is P , expressed in counts per second, the concentration of the associated gamma-ray source in picocuries per gram is

$$\text{concentration} = \frac{27.027}{Y} \cdot I(E) \cdot P , \quad \text{Eq. (4-3)}$$

and the concentration uncertainty is

$$\text{concentration uncertainty} = \frac{27.027}{Y} \cdot I(E) \cdot P \cdot \sqrt{\left(\frac{\sigma I(E)}{I(E)}\right)^2 + \left(\frac{\sigma P}{P}\right)^2} \quad \text{Eq. (4-4)}$$

Y is the gamma-ray yield, in gamma rays per decay, and σP is the uncertainty in the peak intensity. The uncertainty in Y is assumed to be negligible.

4.1.2 Field Verification Criteria

The revised field verification criteria are listed in Tables 2-11, 2-12, and 2-13, all of which are replicated below:

Table 4-2. Field Verification Criteria for Gamma 2A

Gamma-Ray Energy (keV)	Parameter	Lower Control Limit	Upper Control Limit
609.3	Peak intensity	7.731 c/s	9.833 c/s
	FWHM	1.55 keV	2.97 keV
1460.8	Peak intensity	9.209 c/s	10.541 c/s
	FWHM	1.93 keV	3.19 keV
2614.5	Peak intensity	1.988 c/s	2.354 c/s
	FWHM	2.37 keV	3.61 keV

Table 4-3. Field Verification Criteria for Gamma 2B

Gamma-Ray Energy (keV)	Parameter	Lower Control Limit	Upper Control Limit
609.3	Peak intensity	6.426 c/s	10.477 c/s
	FWHM	1.03 keV	3.26 keV
1460.8	Peak intensity	7.965 c/s	12.102 c/s
	FWHM	1.59 keV	3.36 keV
2614.5	Peak intensity	1.660 c/s	2.828 c/s
	FWHM	2.27 keV	3.63 keV

Table 4-4. Field Verification Criteria for Gamma 1D

Gamma-Ray Energy (keV)	Parameter	Lower Control Limit	Upper Control Limit
609.3	Peak intensity	6.481 c/s	8.886 c/s
	FWHM	1.54 keV	2.71 keV
1460.8	Peak intensity	7.105 c/s	9.698 c/s
	FWHM	2.05 keV	2.98 keV
2614.5	Peak intensity	1.514 c/s	2.139 c/s
	FWHM	2.50 keV	3.63 keV

4.1.3 Corrections

4.1.3.1 Dead Time Correction

The dead time correction (DOE 1995) is applied to spectral peak intensities. The correction, which is independent of the gamma-ray energy, is calculated with

$$K_{DT} = \frac{I}{F + G \cdot T_D \cdot \ln(T_D) + H \cdot (T_D)^3} \quad \text{Eq. (4-5)}$$

The dead time correction uncertainty is

$$\sigma K_{DT} = (K_{DT})^2 \cdot \sqrt{(\sigma F)^2 + (T_D \cdot \ln(T_D))^2 \cdot (\sigma G)^2 + (T_D)^6 \cdot (\sigma H)^2} \quad \text{Eq. (4-6)}$$

The dead time effect is assumed to be primarily influenced by the electronics, including the analog-to-digital converter, mounted in the logging vehicle. Therefore, values for the constants in the dead time correction equation are vehicle-dependent. Values for F , G , and H , and their uncertainties, are displayed in Table 4-5.

Table 4-5. Constants for SGLS Dead Time Corrections

Logging Vehicle	$F \pm \sigma F$	$G \pm \sigma G$	$H \pm \sigma H$
Gamma 1 (HO68B3572)	1.0080 ± 0.0054	$(-4.71 \pm 0.47) \times 10^{-4}$	$(-5.73 \pm 0.21) \times 10^{-7}$
Gamma 2 (HO68B3574)	1.0322 ± 0.0022	$(-1.213 \pm 0.028) \times 10^{-3}$	$(-1.89 \pm 0.20) \times 10^{-7}$

If the intensity of a spectral peak is P , with uncertainty σP , then the dead-time-corrected intensity is

$$P \cdot K_{DT} \quad \text{Eq. (4-7)}$$

and the uncertainty in the dead-time-corrected intensity is

$$(P \cdot K_{DT}) \cdot \sqrt{\left(\frac{\sigma P}{P}\right)^2 + \left(\frac{\sigma K_{DT}}{K_{DT}}\right)^2}. \quad \text{Eq. (4-8)}$$

When extreme dead times are due to high concentrations of contaminants with unusually high atomic numbers (Z), the analyst should bear in mind that fluxes of gamma rays with energies less than 500 keV are influenced by the Z effect (Koizumi 1999; Koizumi 2001). An assay based on a low energy gamma ray will produce a spuriously low concentration. The only remedy is to use a peak for a higher energy gamma ray. No correction for the Z effect has been formulated.

4.1.3.2 Tungsten Shield Correction

When zones with high gamma-ray intensities are to be logged, a tungsten shield can be installed on the sonde to reduce the gamma-ray fluxes at the detector (DOE 1995). The shield correction is applied to spectral peak intensities. The correction depends on the gamma-ray energy, E (expressed in kilo-electron-volts):

$$K_{TS} = \exp\left(J + \frac{L \cdot \ln(E) + M}{E^2}\right) \quad \text{Eq. (4-9)}$$

(DOE 1995).

The correction constants are displayed in Table 4-6.

Table 4-6. Constants for the Tungsten Shield Correction

Logging System	$J \pm \sigma J$	$L \pm \sigma L$	$M \pm \sigma M$
Gamma 1A	$(5.750 \pm 0.023) \times 10^{-1}$	$(5.320 \pm 0.093) \times 10^4$	$(-1.33 \pm 0.52) \times 10^4$
Gamma 2D	$(6.170 \pm 0.029) \times 10^{-1}$	$(4.93 \pm 0.12) \times 10^4$	$(1.05 \pm 0.65) \times 10^4$

Shield corrections have not been determined for Detector B. However, if the tungsten shield is used with Detector B, either set of constants could be used to calculate the corrections. As indicated by the entries in Table 4-7, the corrections for Gamma 1A and Gamma 2D are equal, within uncertainties, for gamma-ray energies of interest.

Table 4-7. Examples of Shield Corrections

Gamma-Ray Energy (keV)	Gamma 1A Correction	Gamma 2D Correction
186.0	3739 ± 769	4304 ± 1124
300.0	44.6 ± 3.7	47.4 ± 5.0
400.0	11.99 ± 0.57	12.54 ± 0.76
500.0	6.32 ± 0.20	6.58 ± 0.26
661.6	3.796 ± 0.070	3.945 ± 0.092
1173.2	2.313 ± 0.015	2.406 ± 0.020
1332.5	2.188 ± 0.012	2.277 ± 0.015
1500.0	2.100 ± 0.009	2.186 ± 0.012
1764.5	2.011 ± 0.007	2.093 ± 0.010

The uncertainty in a calculated correction is

$$\sigma K_{TS} = K_{TS} \cdot \sqrt{(\sigma J)^2 + \left(\frac{\ln(E)}{E^2} \cdot \sigma L \right)^2 + \left(\frac{\sigma M}{E^2} \right)^2} . \quad \text{Eq. (4-10)}$$

If the intensity of a spectral peak is P , with uncertainty σP , then the intensity corrected for the shield effect is

$$P \cdot K_{TS} , \quad \text{Eq. (4-11)}$$

and the uncertainty in the corrected intensity is

$$(P \cdot K_{TS}) \cdot \sqrt{\left(\frac{\sigma P}{P} \right)^2 + \left(\frac{\sigma K_{TS}}{K_{TS}} \right)^2} . \quad \text{Eq. (4-12)}$$

4.1.3.3 Casing Corrections

The casing correction is defined as

$$\text{correction} = K_C = \frac{\text{spectral peak intensity from measurement without casing}}{\text{spectral peak intensity from measurement with casing}} . \quad \text{Eq. (4-13)}$$

If a spectral peak has intensity P , then the intensity corrected for the casing effect is

$$P \cdot K_C . \quad \text{Eq. (4-14)}$$

If σP is the uncertainty in P , the uncertainty in the corrected intensity is

$$(P \cdot K_C) \cdot \sqrt{\left(\frac{\sigma P}{P}\right)^2 + \left(\frac{\sigma K_C}{K_C}\right)^2}. \quad \text{Eq. (4-15)}$$

The casing corrections were reformulated in 2001, as described in Appendix A. The revised correction equation is

$$K_C = \exp\left(Q_A + Q_B \cdot E + \frac{Q_C}{E}\right). \quad \text{Eq. (4-16)}$$

E is the gamma-ray energy, expressed in kilo-electron-volts, and Q_A , Q_B , and Q_C are fitting parameters. Each of the fitting parameters is linearly related to the casing thickness, T . For T expressed in inches, the fitting parameters and their uncertainties are

$$\begin{aligned} Q_A &= -0.022 + 1.241 \cdot T, \\ \sigma Q_A &= \sqrt{(0.037)^2 + (0.054 \cdot T)^2}; \\ Q_B &= 1.17 \times 10^{-5} - 0.000213 \cdot T, \\ \sigma Q_B &= \sqrt{(0.77 \times 10^{-5})^2 + (0.000011 \cdot T)^2}; \\ Q_C &= 17.2 + 353.2 \cdot T, \text{ and} \\ \sigma Q_C &= \sqrt{(11.1)^2 + (17.6 \cdot T)^2}. \end{aligned}$$

The uncertainty in the correction is

$$\sigma K_C = K_C \cdot \sqrt{(\sigma Q_A)^2 + (E \cdot \sigma Q_B)^2 + \left(\frac{\sigma Q_C}{E}\right)^2}. \quad \text{Eq. (4-17)}$$

The results in this section are applicable to data acquired with any SGLS sonde.

4.1.3.4 Corrections for Water-Filled Boreholes

The water-filled borehole correction is defined as

$$correction = K_W = \frac{\text{spectral peak intensity from measurement without water}}{\text{spectral peak intensity from measurement with water}}. \quad \text{Eq. (4-18)}$$

If a spectral peak has intensity P , then the intensity corrected for the water effect is

$$P \cdot K_W . \quad \text{Eq. (4-19)}$$

If σP is the uncertainty in P , and σK_W is the uncertainty in K_W , then the uncertainty in the corrected intensity is

$$(P \cdot K_W) \cdot \sqrt{\left(\frac{\sigma P}{P}\right)^2 + \left(\frac{\sigma K_W}{K_W}\right)^2} . \quad \text{Eq. (4-20)}$$

The water-filled borehole corrections were reformulated in 2001, as described in Appendix B. The revised correction equation is

$$K_W = \exp\left(W_A + W_B \cdot E + \frac{W_C}{E}\right), \quad \text{Eq. (4-21)}$$

in which E is the gamma-ray energy, expressed in kilo-electron-volts, and the fitting parameters W_A , W_B , and W_C depend on the borehole diameter, D (expressed in inches), as follows:

$$\begin{aligned} W_A &= \left(1.406 - \frac{4.51}{D}\right)^2, \\ \sigma W_A &= 2 \cdot \sqrt{W_A} \cdot \sqrt{(0.058)^2 + \left(\frac{0.37}{D}\right)^2}; \\ W_B &= -0.000307 + \frac{0.00124}{D}, \\ \sigma W_B &= \sqrt{(0.00043)^2 + \left(\frac{0.00022}{D}\right)^2}; \\ W_C &= \frac{D}{0.168 - 0.0097 \cdot D}, \text{ and} \\ \sigma W_C &= W_C^2 \cdot \sqrt{(0.0046)^2 + \left(\frac{0.051}{D}\right)^2}. \end{aligned}$$

Equation (4-21) expresses the correction in terms of these parameters. The uncertainty in the correction is

$$\sigma K_W = K_W \cdot \sqrt{(\sigma W_A)^2 + (E \cdot \sigma W_B)^2 + \left(\frac{\sigma W_C}{E}\right)^2} . \quad \text{Eq. (4-22)}$$

All of the correction data were acquired with the sonde centered in the calibration standard test holes, and, consequently, the corrections are applicable to data acquired with the sonde centered in the borehole.

The results in this section are applicable to data acquired with any SGLS sonde.

4.2 Neutron-Neutron

Gamma 2F (detector serial number H380932510) was calibrated in May 2001 and again in November 2001. The calibrations established the calibration constants, A and B , which relate the count rate, R , to the volume fraction of water, VF :

$$VF = e^A \cdot e^{B \cdot \ln(R)} = e^A \cdot R^B. \quad \text{Eq. (4-23)}$$

Calibrations were determined for two steel casing configurations, 6-in. inner diameter, 0.28-in.-thick wall, and 8-in. inner diameter, 0.32-in.-thick wall. The calibration results are as follows:

May 2001 Calibration

6-in. casing

$$A = -14.77 \pm 1.14$$

$$B = 2.253 \pm 0.198$$

8-in. casing

$$A = -15.902 \pm 0.438$$

$$B = 2.5894 \pm 0.0807$$

Effective period: May 3, 2001 to November 13, 2001.

November 2001 Calibration

6-in. casing

$$A = -14.52 \pm 0.58$$

$$B = 2.203 \pm 0.087$$

8-in. casing

$$A = -15.720 \pm 0.073$$

$$B = 2.546 \pm 0.012$$

Effective period: November 14, 2001 to the date of the next recalibration.

These calibrations are applicable to neutron-neutron count rates measured under the following conditions:

- sonde must be centered in the borehole
- borehole casing parameters must be close to either 6 in. or 8 in.
- sonde must not be immersed in water
- no grout around the borehole casing.

During the calibration measurements, the sonde was surrounded by calibration standard materials that effectively simulated uniform media of infinite extent. Therefore, the calibration equation cannot be expected to yield accurate VG values if the logged media have thin zones or other inhomogeneous configurations.

Variations in the bulk density of the logged medium probably affect readings, but the density effect cannot be measured with the existing standards. The magnitude of the effect may be indicated by P. Couchat's experiments with a moisture gauge (IAEA 1970). For that particular gauge, the change in calculated VF was approximately 0.1 per unit change in specific gravity.

The recorded count rate, and hence, the calculated VF value, will also be affected by variations in the macroscopic thermal neutron absorption cross section of the logged medium, and VF values are calculated under the assumption that the average cross section of the logged medium is nearly identical to the average cross section of the material in the calibration standards.

5.0 Acknowledgements

Ms. R.M. Paxton organized and formatted this report for publication.

Mr. R.G. McCain discovered the SGLS daily efficiency drift and modified the acceptance criteria to take the drift into account. He also analyzed the field verification spectra and formulated the control limits for field verification tests.

6.0 References

- Engelman, R.E., R.E. Lewis, D.C. Stromswold, and J.R. Hearst, 1995. *Calibration Models for Measuring Moisture in Unsaturated Formations by Neutron Logging*, PNL-10801 UC-606, prepared for the U.S. Department of Energy by the Pacific Northwest Laboratory, Richland, Washington.
- Firestone, R.B., 1996. *Table of Isotopes*, Eighth Edition, Vol. 1, John Wiley and Sons, New York.
- Firestone, R.B., 1999. *Table of Isotopes*, Eighth Edition, Vol. 2, John Wiley and Sons, New York.
- Hearst, J.R, and R.C. Carlson, 1994. "A Comparison of the Moisture Gauge and the Neutron Log in Air-Filled Holes," in *Nuclear Geophysics*, Vol. 8, No. 2, Elsevier Science Ltd., Exeter, England.
- Heistand, B.E., and E.F. Novak, 1984. *Parameter Assignments for Spectral Gamma-Ray Borehole Calibration Models*, GJBX-(284), prepared by Bendix Field Engineering Corporation for the U.S. Department of Energy Grand Junction Projects Office, Grand Junction, Colorado.
- International Atomic Energy Agency (IAEA), 1970. *Neutron Moisture Gauges*, IAEA Technical Report Series 112, International Atomic Energy Agency, Vienna.
- Koizumi, C.J., 1981. *Logging Calibration Models for Fission Neutron Sondes*, GJBX-267(81), prepared for the U.S. Department of Energy by Bendix Field Engineering Corporation, Grand Junction, Colorado.
- _____, 1997. *Hanford Tank Farms Vadose Zone Third Biannual Recalibration of Two Spectral Gamma-Ray Logging Systems Used for Baseline Characterization Measurements in the Hanford Tank Farms*, GJO-97-22-TAR GJO-HAN-13, prepared by MACTEC-ERS for the U.S. Department of Energy Grand Junction Office, Grand Junction, Colorado.
- _____, 1999. *Hanford Tank Farms Vadose Zone Base Calibration of a High Rate Logging System for Characterization of Intense Radiation Zones in the Hanford Tank Farms*, GJO-99-118-TAR GJO-HAN-29, prepared by MACTEC-ERS for the U.S. Department of Energy Grand Junction Office, Grand Junction, Colorado.
- _____, 2000. *Hanford Tank Farms Vadose Zone Seventh Recalibration of Spectral Gamma-Ray Logging System Used for Baseline Characterization Measurements in the Hanford Tank Farms*, GJO-2000-142-TAR GJO-HAN-30, prepared by MACTEC-ERS for the U.S. Department of Energy Grand Junction Office, Grand Junction, Colorado.

Koizumi, C.J., 2001. *Hanford Tank Farms Vadose Zone Monitoring Project Initial Calibration of the Radiometric Assessment System*, GJO-2001-237-TAR, prepared by MACTEC-ERS for the U.S. Department of Energy Grand Junction Office, Grand Junction, Colorado.

Steele, W.D., and D.C. George, 1986. *Field Calibration Facilities for Environmental Measurement of Radium, Thorium, and Potassium*, GJ/TMC-01 (Second Edition) UC-70A, prepared by Bendix Field Engineering Corporation for the U.S. Department of Energy Grand Junction Projects Office, Grand Junction, Colorado.

Taylor, J.K., 1987. *Quality Assurance of Chemical Measurements*, Lewis Publishers, Inc., Chelsea, Michigan.

U.S. Department of Energy (DOE), 1995. *Vadose Zone Monitoring Project at the Hanford Tank Farms Calibration of Two Spectral Gamma-Ray Logging Systems for Baseline Characterization Measurements in the Hanford Tank Farms* (Rev. 0), GJPO-HAN-1, prepared by Rust Geotech for the U.S. Department of Energy Grand Junction Projects Office, Grand Junction, Colorado.

_____, 1999. *Hanford Tank Farms Vadose Zone, Sixth Biannual Recalibration of Spectral Gamma-Ray Logging Systems Used for Baseline Characterization Measurements in the Hanford Tank Farms* (Rev. 0), GJO-99-100-TAR GJO-HAN-26, prepared by MACTEC-ERS for the U.S. Department of Energy Grand Junction Office, Grand Junction, Colorado.

Appendix A
Revised Corrections for Steel Casing

A.1 Background

Because calibrations were determined from measurements in uncased holes, log data from cased boreholes must be corrected for the casing effect. At the time of the first (base) calibrations (DOE 1995), the casing correction was defined as

$$\text{correction} = K_C = \frac{\text{spectral peak intensity from measurement without casing}}{\text{spectral peak intensity from measurement with casing}}. \quad \text{Eq. (A-1)}$$

If a spectral peak has intensity P , then the intensity corrected for the casing effect is

$$P \cdot K_C. \quad \text{Eq. (A-2)}$$

If σP is the uncertainty in P , the uncertainty in the corrected intensity is

$$(P \cdot K_C) \cdot \sqrt{\left(\frac{\sigma P}{P}\right)^2 + \left(\frac{\sigma K_C}{K_C}\right)^2}. \quad \text{Eq. (A-3)}$$

Corrections for steel casing were first developed (DOE 1995) from measurements with test casings with thicknesses of 0.25 in., 0.33 in., 0.375 in., and 0.65 in., and, in addition, a thickness of 0.98 in. that was attained by placing the 0.33-in. casing inside of the 0.65-in. casing. From measurements with test casings inside of calibration model test holes, correction values were determined for gamma-ray energies specific to the sources in the calibration model. The equation

$$K_C = \frac{1}{Q_A + \frac{Q_B}{\ln(E)}} \quad \text{Eq. (A-4)}$$

was established by curve fitting to calculate casing correction values for any value of the gamma-ray energy, E . The factors Q_A and Q_B were constants for a given casing thickness. Table A-1 displays the values of Q_A and Q_B that were determined for the five casing thicknesses.

Table A-1. Casing Correction Factors for Specific Casing Thicknesses

Casing Thickness (in.)	Gamma 1A		Gamma 2D	
	$Q_A \pm \sigma Q_A$	$Q_B \pm \sigma Q_B$	$Q_A \pm \sigma Q_A$	$Q_B \pm \sigma Q_B$
0.25	1.492 ± 0.0038	-5.571 ± 0.023	1.5148 ± 0.0080	-5.768 ± 0.048
0.33	1.5213 ± 0.0031	-6.283 ± 0.018	1.4628 ± 0.0049	-5.928 ± 0.029
0.375	1.5098 ± 0.0037	-6.355 ± 0.022	1.4777 ± 0.0050	-6.179 ± 0.029
0.65	1.2214 ± 0.0061	-5.802 ± 0.034	1.2051 ± 0.0061	-5.711 ± 0.034
0.98	0.879 ± 0.013	-4.460 ± 0.074	0.836 ± 0.014	-4.206 ± 0.078

Hanford monitoring boreholes have casings with thicknesses of 0.28 in., 0.32 in., and other

values different from those represented in the casing measurements. Several methods were developed to calculate corrections for these thicknesses (Koizumi 1997; Koizumi 2000). In the method described by Koizumi (2000), Q_A and Q_B values are calculated by linear interpolation. For example, the Q_A and Q_B values for 0.25-in. and 0.33-in. casing in Table A-1 would be used to calculate the values of Q_A and Q_B for the intermediate thickness of 0.28 in., assuming that the Q_A and Q_B are linear functions of thickness, T , between $T = 0.25$ in. and $T = 0.33$ in.

The linear interpolation method was satisfactory for most casings in monitoring boreholes, but the method's downfall came with the logging of recently installed groundwater sampling wells that have casings with thicknesses exceeding 1 in. The Q_A and Q_B values for these thick casings had to be estimated by *extrapolation*. Whereas extrapolation itself was risky, the resulting Q_A and Q_B values introduced a mathematical catastrophe. The Q_A and Q_B values caused singularities in Equation (A-4); that is, the denominator of the expression on the right side of Equation (A-4) could be zero for certain combinations of casing thickness and gamma-ray energy.

A.2 Revised Steel Casing Corrections

To overcome the problems described in Section A.1, the casing corrections were completely revamped in 2001. The changes were implemented in two steps.

First, the separate corrections for Gamma 1A and Gamma 2D were combined. The method is illustrated with the corrections for the 0.25-in.-thick casing, which happens to be close to the most common monitoring borehole casing thickness (0.28 in.) at Hanford. In Figure A-1, circular symbols show the measured discrete-energy Gamma 1A casing corrections plotted in relation to gamma-ray energy, and triangular symbols show the Gamma 2D corrections similarly plotted. In general, the Gamma 1A corrections are systematically higher than the Gamma 2D corrections, but the differences are small and the separate corrections could be replaced with average corrections without significantly degrading the accuracy.

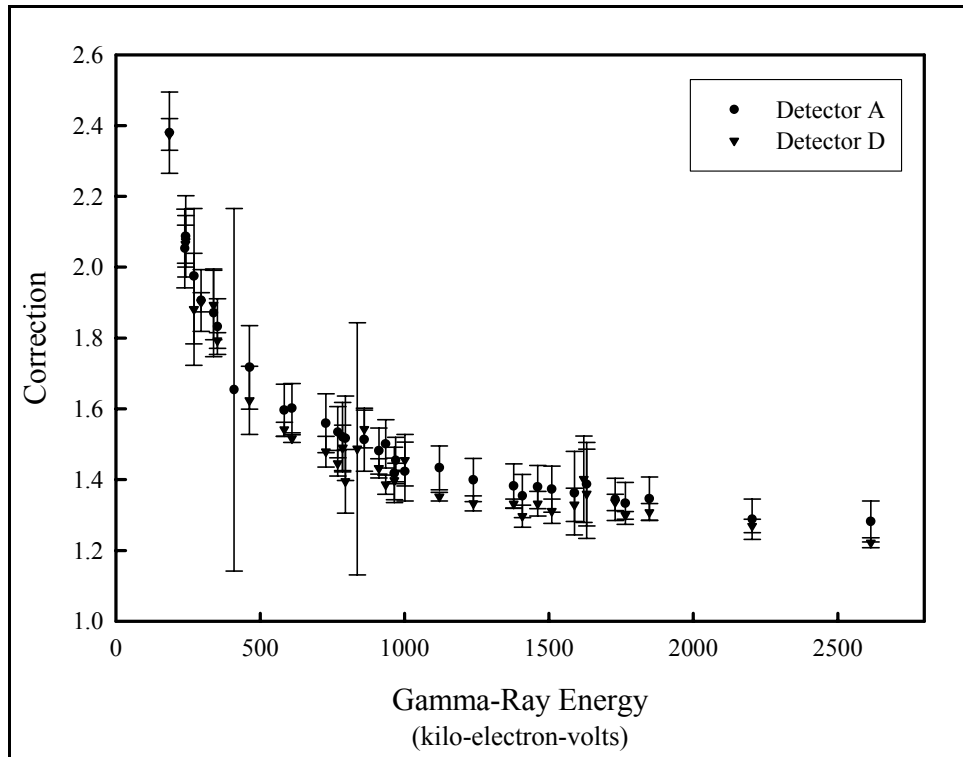


Figure A-1. SGLS 0.25-in. Casing Correction Data

For the determination of average corrections, the ordinary average of the two system corrections at each energy was used. Weighted averages were not used because in general, the Gamma 1A corrections have significantly larger uncertainties than the Gamma 2D corrections. Consequently, if a weight for each correction had been calculated by

$$\text{weight} = \left(\frac{\text{correction}}{\text{uncertainty}} \right)^2, \quad \text{Eq. (A-5)}$$

the Gamma 1A corrections would have had small weights and would have contributed very little to the weighted averages.

The average correction at each discrete energy was taken to be:

$$\text{average correction} = \frac{(\text{Gamma 1A correction} + \text{Gamma 2D correction})}{2}. \quad \text{Eq. (A-6)}$$

If σ_{1A} and σ_{2A} were the uncertainties in the two corrections, then

$$\text{uncertainty} = \frac{\sqrt{(\sigma_{1A})^2 + (\sigma_{2A})^2}}{2} \quad \text{Eq. (A-7)}$$

was used as the uncertainty in the average correction. The average corrections and their uncertainties were analyzed with a curve-fitting program. The function representing the average corrections in relation to gamma-ray energy is plotted, along with the Gamma 1A and Gamma 2D correction data, in Figure A-2.

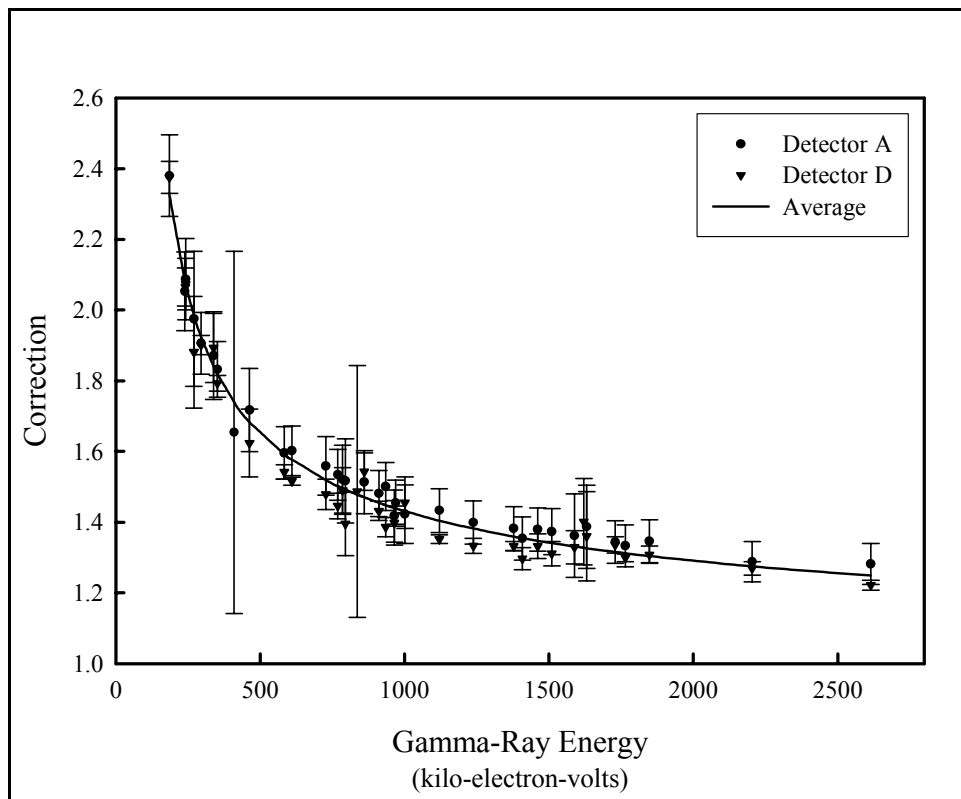


Figure A-2. SGLS 0.25-in. Casing Correction Data with Curve Representing Average Corrections

The plots in the figure indicate that the correction function derived from average correction values represents all of the data reasonably well.

Table A-2 displays measured and calculated corrections at representative gamma energies for both detectors and the 0.25-in.-thick casing. The calculated corrections were determined using the original correction function (Equation (A-4)) and the Q_A and Q_B values derived through curve fitting.

Table A-2. Measured and Calculated Steel Casing Corrections

Gamma-Ray Energy, E (keV)	Calculated Average Correction	Gamma 1A		Gamma 2D	
		Measured Correction	Calculated Correction	Measured Correction	Calculated Correction
185.9	2.325 ± 0.032	2.380 ± 0.115	2.348 ± 0.032	2.375 ± 0.045	2.327 ± 0.046
609.3	1.576 ± 0.013	1.602 ± 0.070	1.605 ± 0.013	1.516 ± 0.011	1.547 ± 0.018
1120.3	1.404 ± 0.010	1.433 ± 0.062	1.432 ± 0.010	1.352 ± 0.012	1.372 ± 0.014

1764.5	1.312 ± 0.009	1.333 ± 0.059	1.339 ± 0.009	1.299 ± 0.011	1.279 ± 0.012
661.6	1.549 ± 0.013	see footnote	1.577 ± 0.013	see footnote	1.519 ± 0.018
1001.0	1.431 ± 0.011	see footnote	1.459 ± 0.011	see footnote	1.399 ± 0.014
1173.2	1.393 ± 0.010	see footnote	1.421 ± 0.010	see footnote	1.361 ± 0.014
1332.5	1.366 ± 0.009	see footnote	1.393 ± 0.010	see footnote	1.334 ± 0.013

Note: The sources for the 661.6-keV (^{137}Cs), 1001.0-keV (processed ^{238}U), 1173.2-keV (^{60}Co), and 1332.5-keV (^{60}Co) gamma rays are not present in the calibration standards. The calculated corrections for these gamma rays are displayed because the sources are frequently encountered at Hanford.

Table A-3 has the same layout as Table A-2, but the “Gamma 1A” and “Gamma 2D” columns show the percent differences between the analogous cell entries in Table A-2 and the calculated average corrections in column 2.

Table A-3. Discrepancies in Corrections

Gamma-Ray Energy, E (keV)	Calculated Average Correction	Gamma 1A		Gamma 2D	
		% Difference, Measured Correction	% Difference, Calculated Correction	% Difference, Measured Correction	% Difference, Calculated Correction
185.9	2.325 ± 0.032	2.4	1.0	2.2	0.09
609.3	1.576 ± 0.013	1.7	1.8	-3.8	-1.8
1120.3	1.404 ± 0.010	2.0	2.0	-3.7	-2.3
1764.5	1.312 ± 0.009	1.6	2.1	-1.0	-2.5
661.6	1.549 ± 0.013		1.8		-1.9
1001.0	1.431 ± 0.011		2.0		-2.2
1173.2	1.393 ± 0.010		2.0		-2.3
1332.5	1.366 ± 0.009		2.0		-2.3

The small percent differences in Table A-3 indicate that the calculated average corrections accurately represent the actual corrections.

Similar results were obtained for the other thicknesses. For example, Figure A-3 shows 0.65-in.-thick casing results in the same format as Figure A-2.

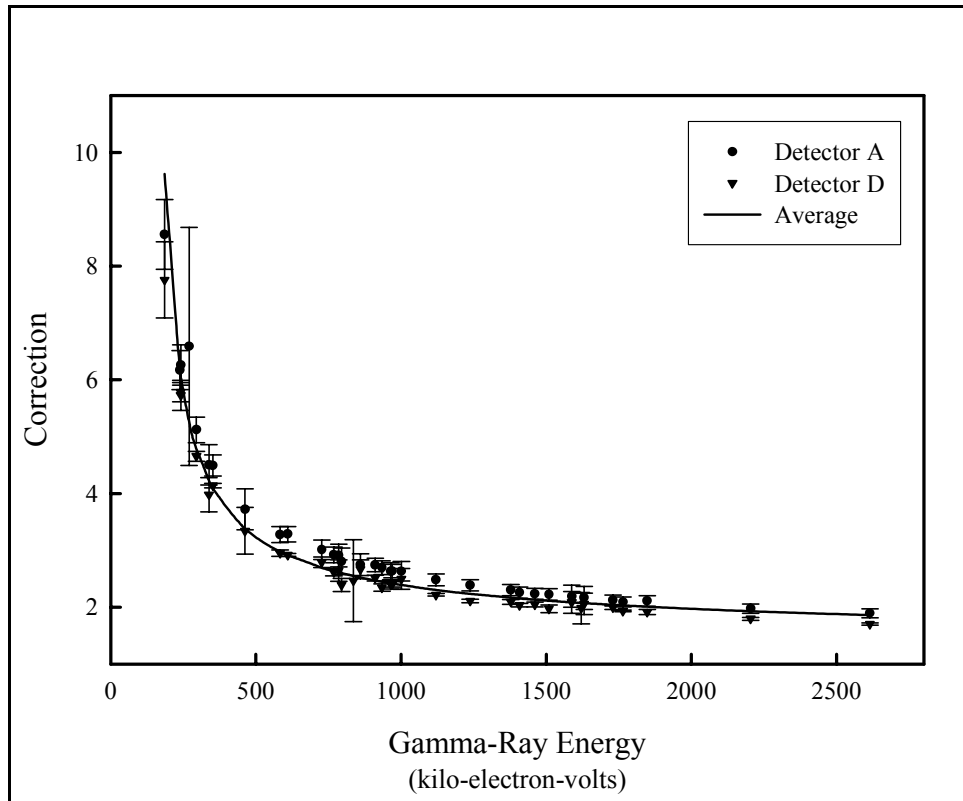


Figure A-3. SGLS 0.65-in. Casing Correction Data with Curve Representing Average Corrections

Again, the calculated average corrections accurately represent the actual corrections.

After the average corrections for the various discrete energies and discrete casing thicknesses (0.25, 0.33, 0.375, 0.65, and 0.98 in.), were calculated, the second step of the casing correction reformulation was undertaken. The average corrections were analyzed with the curve fitting program to determine a new equation to express the correction as a function of gamma-ray energy:

$$K_C = \exp\left(Q_A + Q_B \cdot E + \frac{Q_C}{E}\right). \quad \text{Eq. (A-8)}$$

E is the gamma-ray energy, expressed in kilo-electron-volts, and Q_A , Q_B , and Q_C are the fitting parameters. The original function (Equation (A-4)) had two fitting parameters, whereas the proposed replacement (Equation (A-8)) has three fitting parameters.

After the curve fitting program was used to calculate values of Q_A , Q_B , and Q_C for the discrete casing thicknesses of 0.25, 0.33, 0.375, 0.65, and 0.98 in., the calculated corrections could be compared with the average corrections. Examples of these comparisons are shown in Figures A-4, A-5, and A-6.

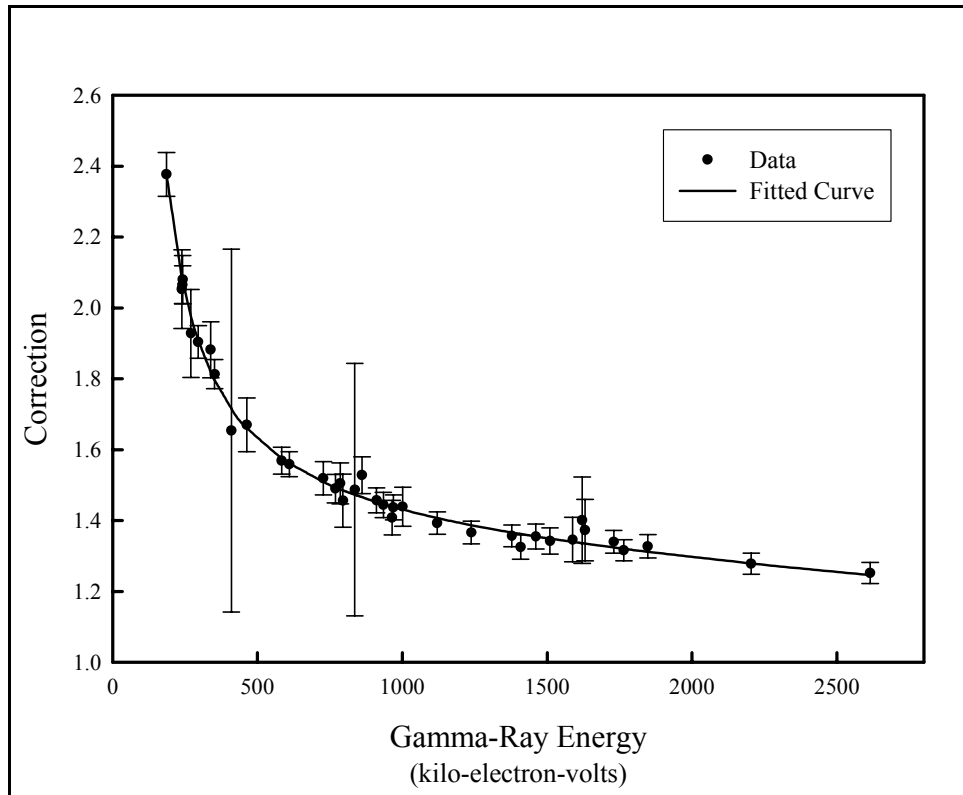


Figure A-4. Corrections for the 0.25-in.-Thick Casing

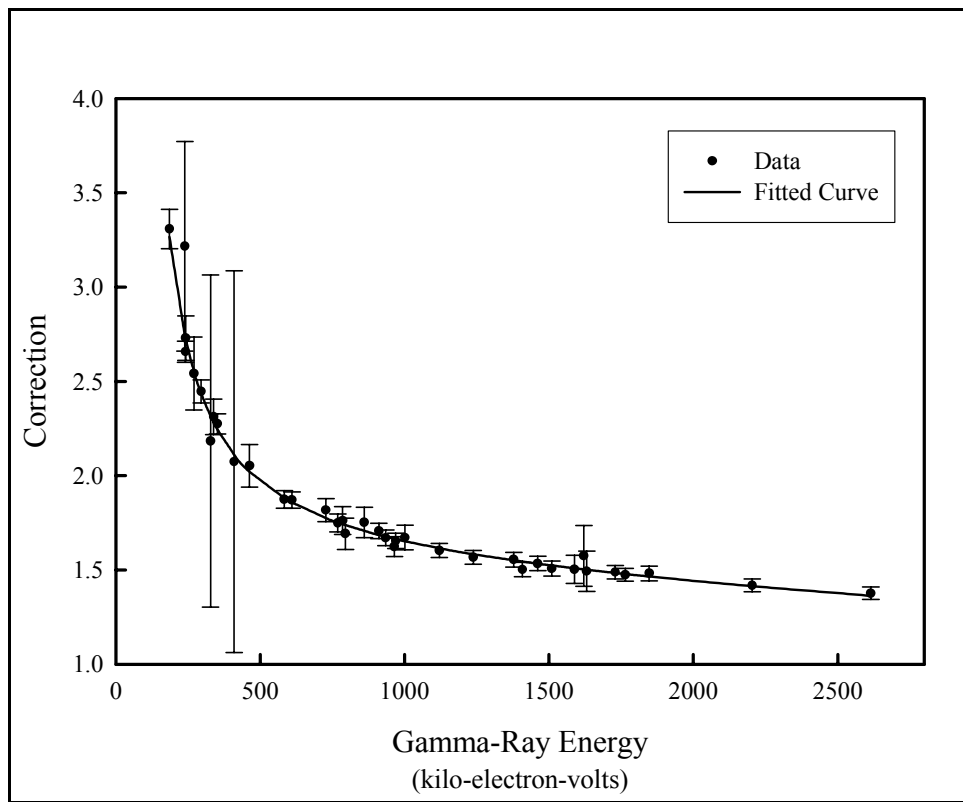


Figure A-5. Corrections for the 0.375-in.-Thick Casing

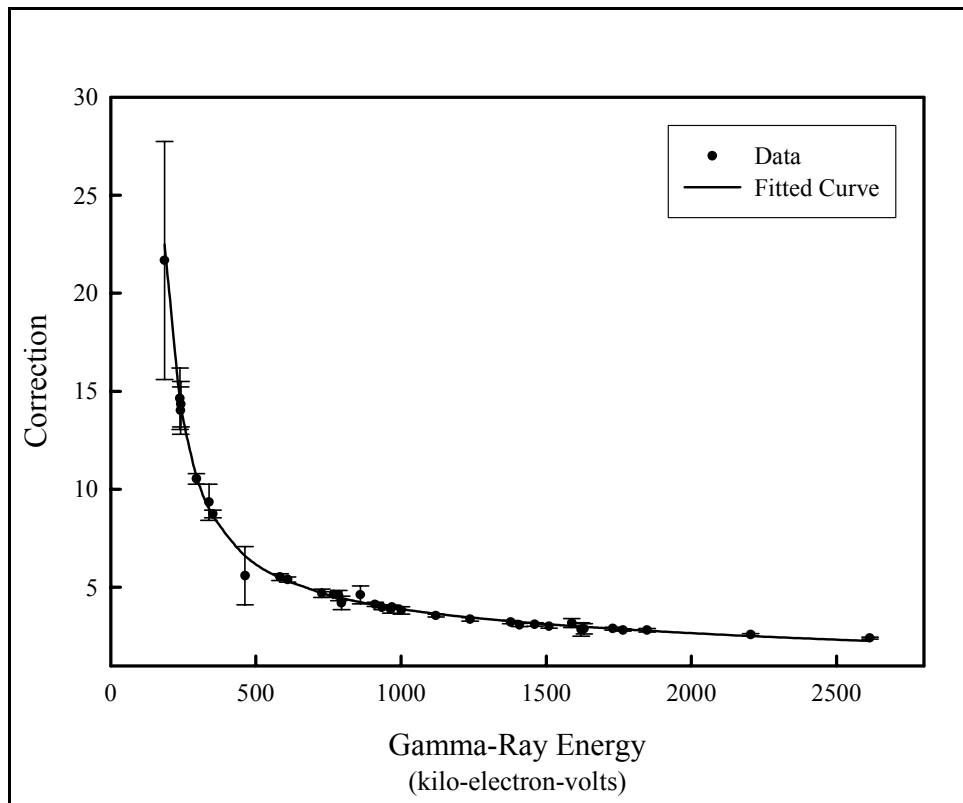


Figure A-6. Corrections for the 0.98-in.-Thick Casing

Equation (A-8) obviously provides excellent fits to data. The fits at energies higher than about 1300 keV are particularly superior to the fits provided by Equation (A-4). Corrections calculated with Equation (A-4) were systematically higher than the measured corrections, as indicated by the plots in Figure 8-1 of the base SGLS calibration report (GJO-HAN-1, August 1995).

Another advantage of Equation (A-8) is revealed by the dependences of the fitting parameters, Q_A , Q_B , and Q_C on the casing wall thickness. These dependences are illustrated by the plots in Figures A-7, A-8, and A-9.

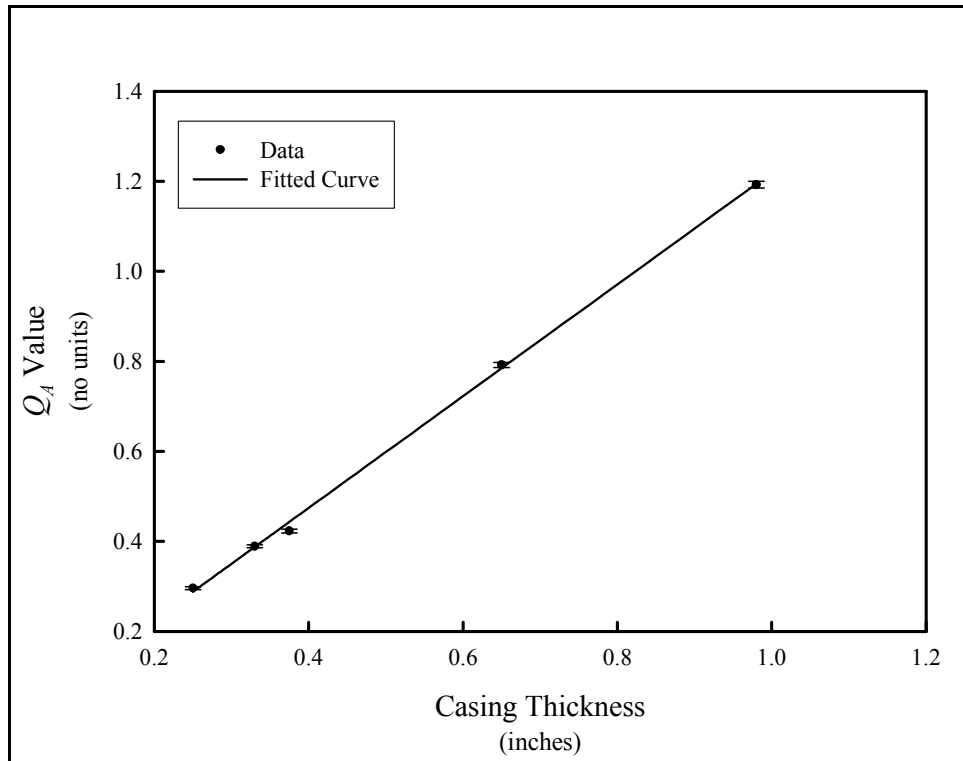


Figure A-7. Plot of the Q_A Values in Relation to Casing Thickness

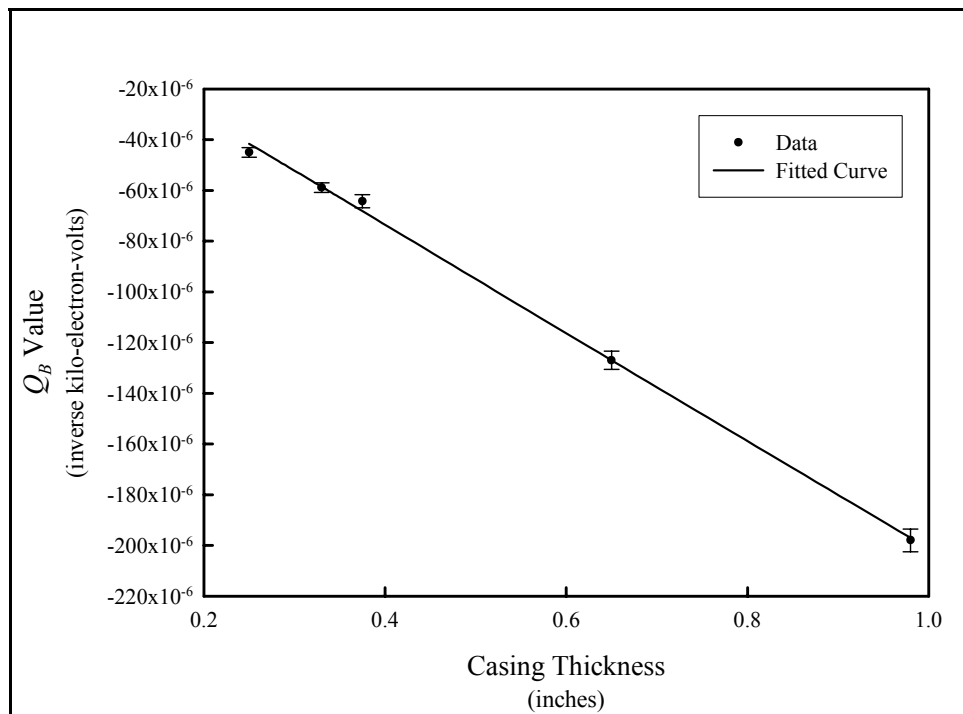


Figure A-8. Plot of the Q_B values in Relation to Casing Thickness

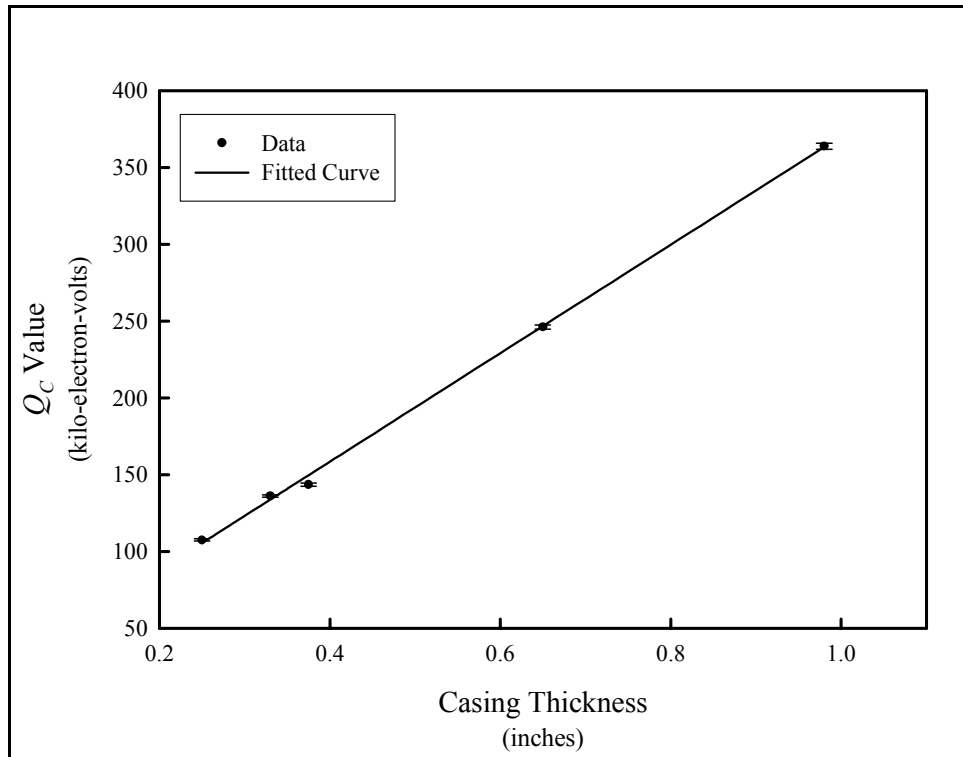


Figure A-9. Plot of the Q_C values in Relation to Casing Thickness

The fitting parameters Q_A , Q_B , and Q_C are linearly related to the casing thickness T :

$$\text{parameter} = \alpha + \beta \cdot T. \quad \text{Eq. (A-9)}$$

α and β have the following values (if T is expressed in inches).

Q_A :

$$\alpha = -0.022 \pm 0.037$$

$$\beta = 1.241 \pm 0.054.$$

Q_B :

$$\alpha = (1.17 \pm 0.77) \times 10^{-5}$$

$$\beta = -0.000213 \pm 0.000011.$$

Q_C :

$$\alpha = 17.2 \pm 11.1$$

$$\beta = 353.2 \pm 17.6.$$

Therefore, the fitting parameters and their uncertainties are

$$Q_A = -0.022 + 1.241 \cdot T,$$

$$\sigma Q_A = \sqrt{(0.037)^2 + (0.054 \cdot T)^2} ;$$

$$Q_B = 1.17 \times 10^{-5} - 0.000213 \cdot T ,$$

$$\sigma Q_B = \sqrt{(0.77 \times 10^{-5})^2 + (0.000011 \cdot T)^2} ;$$

$$Q_C = 17.2 + 353.2 \cdot T , \text{ and}$$

$$\sigma Q_C = \sqrt{(11.1)^2 + (17.6 \cdot T)^2} .$$

Equation (A-8) expresses the correction in terms of these parameters. The uncertainty in the correction is

$$\sigma K_C = K_C \cdot \sqrt{(\sigma Q_A)^2 + (E \cdot \sigma Q_B)^2 + \left(\frac{\sigma Q_C}{E} \right)^2} . \quad \text{Eq. (A-10)}$$

The fact that the Q_A , Q_B , and Q_C values are linearly related to the casing thickness opens the possibility that the Q_A , Q_B , and Q_C values for casing thicknesses greater than 1 in. might be estimated by linear extrapolation. This possibility is of interest because there is no way to experimentally determine corrections for large-thickness casings. Measurements with thick casings cannot be done at Hanford because the diameters of the test holes in the Hanford calibration standards are too small.

Because measurements are not possible, results obtained by extrapolation cannot be confirmed. However, evidence that such results are plausible can be acquired. The second and third columns of Table A-4 display corrections for the 0.65-in. and 0.98-in. thicknesses that were calculated using Equation (A-8) and the appropriate Q_A , Q_B , and Q_C values. These corrections are accurate, as demonstrated by the plot in Figure A-6 for the 0.98-in.-thick casing. For any energy, the correction for a 1.63-in.-thick casing could be estimated by multiplying the 0.65-in. correction by the 0.98-in. correction. The fourth column in the table shows corrections that were calculated this way. The fifth column shows the corrections that were calculated using Equation (A-8) and the Q_A , Q_B , and Q_C values derived by extrapolating the curves in Figures A-7, A-8, and A-9 to the thickness 1.63 in.

Table A-4. Estimates of Casing Corrections for a 1.63-in.-Thick Casing

Energy (keV)	0.65-in. Correction Calculated With Eq. (A-8)	0.98-in. Correction Calculated With Eq. (A-8)	Product of 0.65-in. Correction and 0.98-in. Correction	1.63-in. Correction Calculated With Eq. (A-8)
200	7.34	19.53	143.40	134.19
300	4.81	10.45	50.24	48.33
400	3.86	7.58	29.27	28.53
500	3.37	6.20	20.90	20.52
600	3.07	5.38	16.52	16.29

Energy (keV)	0.65-in. Correction Calculated With Eq. (A-8)	0.98-in. Correction Calculated With Eq. (A-8)	Product of 0.65-in. Correction and 0.98-in. Correction	1.63-in. Correction Calculated With Eq. (A-8)
800	2.70	4.45	12.02	11.91
1000	2.48	3.91	9.68	9.61
1200	2.32	3.54	8.20	8.15
1400	2.20	3.26	7.16	7.11
1600	2.09	3.04	6.36	6.31
1800	2.01	2.85	5.72	5.67
2000	1.93	2.68	5.19	5.14
2200	1.86	2.54	4.73	4.68
2400	1.80	2.41	4.34	4.28
2600	1.74	2.29	3.99	3.93
2800	1.69	2.18	3.68	3.62

The correction values in columns 4 and 5 of Table A-4 are plotted in relation to gamma-ray energy in Figure A-10.

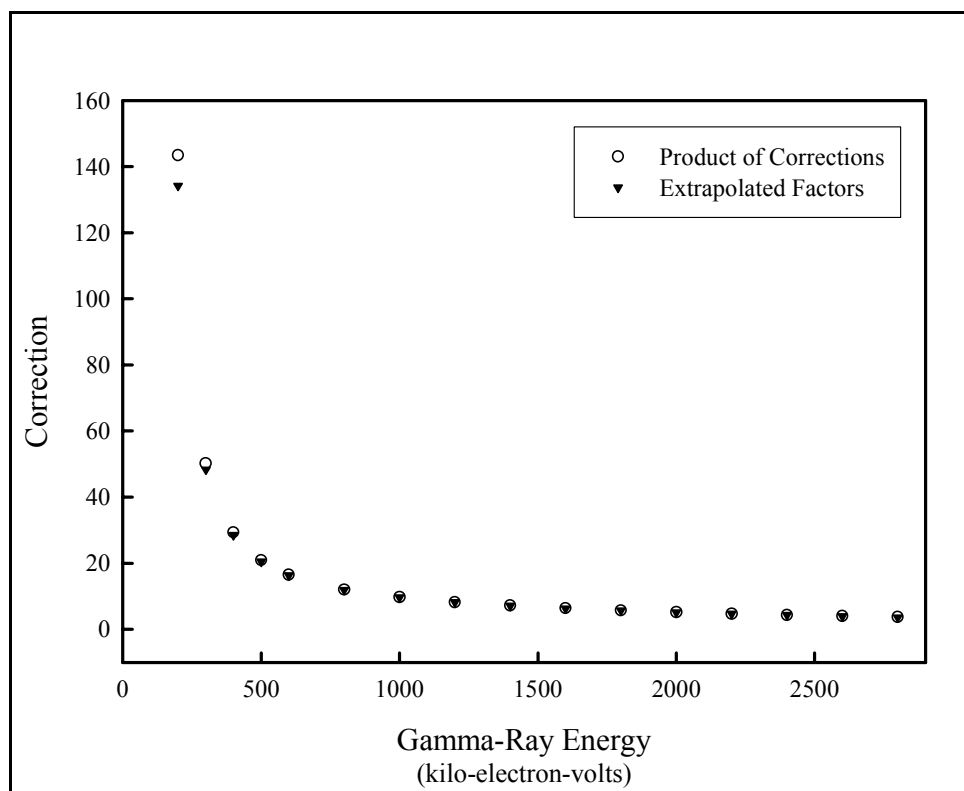


Figure A-10. "Product of Corrections" Values Calculated by Multiplying the 0.65-in. Corrections by the 0.98-in. Corrections; "Extrapolated Factors" Corrections Calculated by Extrapolating the Q_A , Q_B , and Q_C Values to the 1.63-in. Thickness, then using Equation (A-8)

The physics of casing attenuation (DOE 1995) indicates that the product of corrections for two thicknesses, T_1 and T_2 , should be slightly greater than the actual correction for the thickness ($T_1 +$

T₂), but that the differences should diminish as the energy increases. The results in Table A-4 and Figure A-10 conform to these principles (for energies below 2000 keV, at least). These observations do not prove that the 1.63-in. corrections in the fifth column of Table A-4 are correct, but they make the corrections plausible.

Casing data recorded with Detectors A and D were combined to derive the results in this section, and the results are applicable to data acquired with any SGLS sonde.

Obviously, this method should not be used to extrapolate to thicknesses exceeding 1.63 in. until further investigation indicates the upper limits of the method.

Appendix B
Revised Corrections for Water-Filled Boreholes

B.1 Background

Development of corrections for water-filled boreholes followed a path similar to that which led to the casing corrections (DOE 1995). The correction was defined as

$$\text{correction} = K_W = \frac{\text{spectral peak intensity from measurement without water}}{\text{spectral peak intensity from measurement with water}}. \quad \text{Eq. (B-1)}$$

If a spectral peak has intensity P , then the intensity corrected for the water effect is

$$P \cdot K_W. \quad \text{Eq. (B-2)}$$

If σP is the uncertainty in P , and σK_W is the uncertainty in K_W , then the uncertainty in the corrected intensity is

$$(P \cdot K_W) \cdot \sqrt{\left(\frac{\sigma P}{P}\right)^2 + \left(\frac{\sigma K_W}{K_W}\right)^2}. \quad \text{Eq. (B-3)}$$

The first water-filled borehole corrections were determined for the specific borehole diameters of 4.5, 7.0, 9.0, and 12 inches (DOE 1995). Although measurements were conducted with Gamma 1A and Gamma 2D, it was subsequently determined that the Gamma 1A data were affected by an electrical problem in the sonde (DOE 1995, DOE 1999) that apparently influenced measurements only when the sonde was immersed in water. Corrections were therefore derived using only the Gamma 2D data. Later, Koizumi (2000) showed that the corrections determined with the method can be applied to data recorded with Gamma 1A.

Analysis of the Gamma 2D data with a curve-fitting program indicated that the correction for a particular energy E (expressed in kilo-electron-volts) could be calculated with

$$K_W = \sqrt{W_A + \frac{W_B}{E}}, \quad \text{Eq. (B-4)}$$

in which W_A and W_B were parameters determined by curve fitting.

Because few, if any, of the Hanford boreholes have diameters matching those for which corrections were determined, general methods were developed to calculate corrections. Koizumi (2000) developed a linear interpolation method to calculate W_A and W_B values. If the values for W_{A1} and W_{B1} and W_{A2} and W_{B2} were known for two particular borehole diameters D_1 and D_2 (expressed in inches), then the W_A and W_B values for a borehole of intermediate diameter D ($D_1 < D < D_2$) would be calculated by linear interpolation:

$$W_A = \left(1 - \frac{D - D_1}{D_2 - D_1}\right) \cdot W_{A1} + \left(\frac{D - D_1}{D_2 - D_1}\right) \cdot W_{A2} \quad \text{Eq. (B-5)}$$

and

$$W_B = \left(1 - \frac{D - D_1}{D_2 - D_1}\right) \cdot W_{B1} + \left(\frac{D - D_1}{D_2 - D_1}\right) \cdot W_{B2} . \quad \text{Eq. (B-6)}$$

B.2 Revised Water-Filled Borehole Corrections

As was done with casing corrections, the linear interpolation method was recently replaced. Re-analysis of the Detector D data with the curve fitting program indicated that the water corrections can be represented with the same equation (Equation (A-8)) as used for the casing corrections:

$$K_W = \exp\left(W_A + W_B \cdot E + \frac{W_C}{E}\right). \quad \text{Eq. (B-7)}$$

E is the gamma-ray energy, expressed in kilo-electron-volts, and the fitting parameters W_A , W_B , and W_C have constant values for a given borehole diameter.

The water correction parameters are not linearly related to the borehole diameter. However, the relationships are simple:

$$W_A = \left(1.406 - \frac{4.51}{D}\right)^2,$$

$$\sigma W_A = 2 \cdot \sqrt{W_A} \cdot \sqrt{(0.058)^2 + \left(\frac{0.37}{D}\right)^2};$$

$$W_B = -0.000307 + \frac{0.00124}{D},$$

$$\sigma W_B = \sqrt{(0.00043)^2 + \left(\frac{0.00022}{D}\right)^2};$$

$$W_C = \frac{D}{0.168 - 0.0097 \cdot D},$$

$$\sigma W_C = W_C^2 \cdot \sqrt{(0.0046)^2 + \left(\frac{0.051}{D}\right)^2}.$$

In the equations above, D must be expressed in inches.

Equation (B-7) expresses the correction in terms of these parameters. The uncertainty in the correction is

$$\sigma K_W = K_W \cdot \sqrt{(\sigma W_A)^2 + (E \cdot \sigma W_B)^2 + \left(\frac{\sigma W_C}{E}\right)^2}. \quad \text{Eq. (B-8)}$$

All of the correction data were acquired with the sonde centered in the calibration standard test holes, and, consequently, the corrections are applicable to data acquired with the sonde centered in the borehole.

These results are applicable to data acquired with any SGLS sonde.